95 GeV diphoton and $b\bar{b}$ excesses in the general next-to-minimal supersymmetric standard model

Junjie Cao,[1,2,*] Xinglong Jia,[1,†] Jingwei Lian,[3,‡] and Lei Meng[1,§]

[1]School of Physics, Henan Normal University, Xinxiang 453007, China
[2]School of Physics, Shandong University, Jinan, Shandong 250100, China
[3]Henan Institute of Science and Technology, Xinxiang 453003, China

(Received 20 October 2023; accepted 8 March 2024; published 3 April 2024)

The CMS and ATLAS Collaborations recently published their results searching for light Higgs bosons, using the complete Run 2 data of the LHC. Both reported an excess in the diphoton invariant mass distribution at $m_{\gamma\gamma} \simeq 95.4$ GeV with compatible signal strengths. The combined result corresponded to a local significance of 3.1σ. Besides, the mass of the diphoton signal coincided with that of the $b\bar{b}$ excess observed at the Large Electron Positron. Given the remarkable theoretical advantages of the general next-to-minimal supersymmetric Standard Model, we interpret these excesses by the resonant productions of the singlet-dominated *CP*-even Higgs boson predicted by the theory. Using both analytic formulas and numerical results, we show that the idea can interpret the excesses by broad parameter space without contradicting current experimental restrictions, including those from the 125 GeV Higgs data, the dark matter relic abundance and direct detection experiments, and the collider searches for supersymmetry and extra Higgs bosons. Although the explanations are scarcely affected by present Higgs data and the LHC search for supersymmetry, the dark matter physics may leave footprints on them. We also survey the other signals of the light Higgs boson at the LHC.

DOI: 10.1103/PhysRevD.109.075001

I. INTRODUCTION

The discovery of the Higgs boson at the Large Hadron Collider (LHC) in 2012 proved the existence of a scalar field. It provided essential insights into the electroweak symmetry breaking (EWSB) and mass generation mechanisms. Although the properties of this boson are consistent with the predictions of the Standard Model (SM), the notorious hierarchy problem implies that the SM might not be the whole story, and there ought to be a more underlying framework from physics beyond the SM (BSM) to account for the EWSB. Since the BSM physics often gives rise to extended Higgs sectors in which additional scalar particles are present, searching for extra Higgs bosons becomes one of the primary objectives of the LHC. In this regard, it is noticeable that the presence of additional scalars with masses below 125 GeV is not excluded if their couplings are suppressed compared to those of the SM Higgs boson. These extra Higgs bosons are within the reach of the LHC, and with moderately large couplings, they would have been produced in small numbers in past runs. Thus, an intriguing question is whether there could be hints of one or more additional Higgs bosons in the currently existing searches in the form of no-significant excesses over the background expectation.

Among the ongoing searches for low-mass Higgs bosons, the CMS Collaboration first revealed in 2015 an excess with a local significance of 2.0σ in the diphoton invariant-mass distribution at $m_{\gamma\gamma} \simeq 97$ GeV, based on 19.7 fb^{-1} of LHC data at a center-of-mass energy of 8 TeV [1]. This excess was reinforced to 2.8σ in 2018 at $m_{\gamma\gamma} \simeq 95$ GeV after combining the Run 1 data and 35.9 fb^{-1} of LHC data at 13 TeV [2]. Remarkably, CMS released its latest analysis in March 2023, confirming the excess at $m_{\gamma\gamma} = 95.4$ GeV and with a local significance of 2.9σ by employing advanced analysis techniques and utilizing data collected during the first, second, and third years of Run 2, which correspond to integrated luminosities of 36.3 fb^{-1}, 41.5 fb^{-1}, and 54.4 fb^{-1}, respectively, with a shared collision energy of 13 TeV [3]. By contrast, the observations of the ATLAS Collaboration are somewhat different. Specifically, this collaboration did not find a significant excess around 95 GeV after scrutinizing 80 fb^{-1} of LHC data in 2018 [4]. However, given that its sensitivity was minor, its limits

*junjiec@alumni.itp.ac.cn
†JiaXinglong1996@outlook.com
‡lianjw@hist.edu.cn
§mel18@foxmail.com

on the diphoton production rate were not in tension with the CMS results. Encouragingly, the collaboration recently released its analysis in searching for the diphoton resonances in the mass range from 66 GeV to 110 GeV using the full Run 2 LHC dataset (140 fb^{-1}) [5]. Compared with its previous one [4], using multivariate analysis techniques in background mitigation and event classification improved the sensitivity to BSM physics. Numerically speaking, this further analysis revealed an excess in the diphoton channel at an invariant mass around 95 GeV and with a local significance of 1.7σ, remarkably aligning with the reported CMS findings.

Regarding interpreting the new result from ATLAS and the previously reported ones from CMS, one should note that the observed diphoton events at about 95 GeV might originate from fluctuating a much more extensive background, thus giving rise to a relatively small number of pseudosignals. Therefore, one cannot necessarily expect that the excesses should occur with the same signal strength. In this context, the phenomenon that both collaborations reported their most significant excess at the same mass value has to be seen as a certain level of coincidence. However, since for the same mass value, the renormalized diphoton production rates revealed by the two collaborations, namely $\mu_{\gamma\gamma}^{\rm CMS} = 0.33^{+0.19}_{-0.12}$ and $\mu_{\gamma\gamma}^{\rm ATLAS} = 0.18 \pm 0.10$, agree with each other within their uncertainties, it is intriguing to imagine that they arise from the production of a single new particle. If it proves true, this will be the first sign of new physics in the Higgs-boson sector [6]. With this assumption, one could obtain a combined signal strength after neglecting possible correlations. It is given by [6]

$$\mu_{\gamma\gamma}^{\rm exp} \equiv \mu_{\gamma\gamma}^{\rm ATLAS+CMS} = \frac{\sigma(pp \to \phi \to \gamma\gamma)}{\sigma_{\rm SM}(pp \to H_{\rm SM} \to \gamma\gamma)} = 0.24^{+0.09}_{-0.08}, \tag{1.1}$$

where ϕ is a postulated non-Standard scalar with $m_\phi = 95.4$ GeV, responding for the diphoton excess, and $\sigma_{\rm SM}$ denotes the cross section for a hypothetical SM Higgs boson, $H_{\rm SM}$, at the same mass. According to the analysis in Ref. [6], this fitted value corresponds to a 3.1σ local excess. We note that the existence of a light ϕ might also be hinted at by the results of the Large Electron Positron (LEP) in 2006, which showed an excess in the $e^+e^- \to Z\phi(\phi \to b\bar{b})$ mode at $m_{b\bar{b}} \simeq 98$ GeV with a local significance of 2.3σ and $\mu_{b\bar{b}}^{\rm exp} = 0.117 \pm 0.057$ [7–9]. Considering the limited mass resolution for the dijets at LEP, the $b\bar{b}$ excess could originate from the same particle responsible for the diphoton excess summarized above.[1] We also note that $\mu_{\gamma\gamma}^{\rm exp}$ in Eq. (1.1) is much smaller than its previous value $\mu_{\gamma\gamma}^{\rm CMS} = 0.6 \pm 0.2$, derived by the CMS Collaboration from the analysis in 2018 [12]. This situation allows the new particles contributing to the diphoton rate by loop effects to be relatively heavy, consistent with the results of the LHC search for new states.

The appearance of the excesses mentioned above triggered studies on the possibility to accommodate them in BSM models, which predict a SM-like Higgs boson with a mass of around 125 GeV and a lighter nonstandard Higgs boson. These models include the SM extensions with a $SU(2)_L$ triplet scalar field [13] or vectorlike fermions [14–16], the two Higgs-doublet model [17–21] and its extensions with an additional real or complex singlet scalar [6,22–33], Radion model [34], Georgi-Machacek model [35], and the SM extensions within the framework of supersymmetry (SUSY) [9,12,25,36–48]. In addition, there were discussions about possible connections of the observed excesses to extra dimensions [49], B-anomalies [50], dark matter (DM) [51], and neutrino mass generation mechanisms [52,53]. Among these models, the next-to-minimal supersymmetric Standard Model (NMSSM) [54] has attracted significant attention in recent years since it is the most economical supersymmetric theory to account for the diphoton and $b\bar{b}$ excesses [9,12,38,44]. It augments the popular minimal supersymmetric Standard Model (MSSM) with one gauge-singlet Higgs field $\hat{S}$. Like the MSSM, it provides an elegant solution to the hierarchy problem and realizes the unification of gauge interactions at a high energy scale. It is distinct in naturally solving the μ-problem of the MSSM[2] and predicting more feasible DM candidates [63–65]. As a result, the model's phenomenology is significantly enriched [66–70]. In addition, concerning the light CP-even Higgs scenario of the model suited to explain the excesses, the mass of the SM-like Higgs boson may be sizably lifted by both an additional tree-level contribution and the singlet-doublet mixing effect [71–73], which mitigates the significant radiative corrections from top/stop loops needed to predict the SM-like Higgs boson mass at 125 GeV.

We once studied the capability of the NMSSM with a $\mathbb{Z}_3$ discrete symmetry ($\mathbb{Z}_3$-NMSSM) to explain the excesses [9], assuming the singlet-dominated CP-even Higgs boson

[1] Additional hints for the existence of a scalar particle with a mass around 95 GeV include the di-τ excess observed by the CMS collaboration [10], as discussed below, and the WW excess reported in Ref. [11].

[2] In the MSSM, the direct detection of DM by the LUX-ZEPLIN (LZ) experiment [55] alone has required the higgsino mass to be significantly higher than the electroweak scale, namely, $\mu \gtrsim 380$ GeV [56]. Although such a large μ may be generated by the well-known Giudice-Masiero mechanism in the gravity-mediated SUSY breaking scenario [57], it induces severe fine-tuning problems in the light of the LHC Higgs discovery and the absence of any discovery of supersymmetry when the MSSM runs down from an infrared high energy scale to the electroweak scale [58–60]. The NMSSM dynamically generates the μ parameter of the MSSM after the scalar component field of $\hat{S}$ develops a vacuum expectation value (VEV) of $\mathcal{O}(1$ TeV), firstly proposed by P. Fayet [61,62]. In this sense, the NMSSM is a self-contained supersymmetric theory at the electroweak scale.

to be responsible for the diphoton and $b\bar{b}$ excesses. One distinct feature of the $\mathbb{Z}_3$ NMSSM was that there were six input parameters for each of the Higgs sector and the neutralino sector, and four of them, namely λ, κ, $\tan\beta$, and μ, were shared by these two sectors. Consequently, the theory's Higgs and DM physics were entangled. This correlation limited the maximum reach of the diphoton signal rate after including the restrictions from DM experiments and the 125 GeV Higgs data collected at the LHC, so the theory hardly explained the diphoton excess at the 1σ level [9]. Noting that the diphoton rate inferred from the excesses has been reduced significantly, and simultaneously the sensitivities of DM direct detection experiments have been improved by more than 1 order compared with the previous study, we recently renewed the research in Ref. [9]. With the same advanced research strategy as that of this work and the latest relevant experimental results, we found that without finely tuning the model's parameters, the conclusion remained valid, implying the necessity to loosen the correlation to explain the excesses. This situation could be changed by improving the theory in two directions. One was to augment the $\mathbb{Z}_3$ NMSSM with the Type-I or inverse seesaw mechanism to generate neutrino masses and take the gauge-singlet sneutrino as the DM candidate [41]. In this framework, the DM physics was mainly determined by the neutrino Yukawa couplings instead of the parameters in the Higgs sector. As a result, a wide range of parameter spaces in the Higgs sector were resurrected to be experimentally allowed and thus enabled the theory to explain the excesses. The other was, motivated by solving the domain wall and tadpole problems of the $\mathbb{Z}_3$ NMSSM, to neglect the *ad hoc* $\mathbb{Z}_3$ symmetry and consider the general form of the NMSSM, abbreviated as GNMSSM in this work [54]. In the GNMSSM, although the number of the shared parameters in the Higgs and neutralino sectors remained four, the Higgs physics was determined by ten parameters. It thus became more flexible and might account for the excesses. Notably, this characteristic might, in return, enrich the DM properties since the Higgs bosons usually played a role in DM physics.

The excesses in the general NMSSM were analyzed in Ref. [44] by both compact analytic formulas and numerical results. It concluded that there were parameter spaces that could explain the excesses without conflicting with the LHC Higgs data. However, such a study did not specify the singlet self-interactions, which could affect Higgs boson masses, and considered the old results of the diphoton excess. More crucially, it neglected the tight restrictions from the DM physics and the LHC search for supersymmetric particles (sparticles), especially those from the LZ experiment which has reached an unprecedented sensitivity to the cross sections of spin-independent (SI) and spin-dependent (SD) DM-nucleon scatterings, at the level of $10^{-48}\mathrm{cm}^2$ and $10^{-42}\mathrm{cm}^2$, respectively [55]. Given that the NMSSM is one of the most popular supersymmetric theories, such impacts should be included in a comprehensive study of the excesses. This paper will focus on the feasibility of explaining the combined excess in the GNMSSM and its interplay with the latest DM experimental results.

This paper is organized as follows. In Sec. II, we briefly introduce the basic skeleton of the GNMSSM and discuss the signal rates of the $\gamma\gamma$ and $b\bar{b}$ events. In Sec. III, we perform a comprehensive scan over the model parameter space and present the numerical results by both figures and tables. In Sec. IV, we discuss the implications of the excesses. Finally, the conclusion and comments are made in Sec. V.

II. THEORETICAL PRELIMINARIES

A. The basics of GNMSSM

The GNMSSM includes the most general renormalizable couplings in its superpotential, given by [54]

$$W_{\mathrm{GNMSSM}} = W_{\mathrm{Yukawa}} + \lambda\hat{S}\,\hat{H}_u\cdot\hat{H}_d + \frac{\kappa}{3}\hat{S}^3 + \mu\hat{H}_u\cdot\hat{H}_d + \frac{1}{2}\mu'\hat{S}^2 + \xi\hat{S}, \tag{2.1}$$

where W_{Yukawa} contains the quark and lepton Yukawa terms in the MSSM superpotential, $\hat{H}_u = (\hat{H}_u^+, \hat{H}_u^0)^T$ and $\hat{H}_d = (\hat{H}_d^0, \hat{H}_d^-)^T$ are the $SU(2)_L$ doublet Higgs superfields, and $\hat{S}$ is the singlet Higgs superfield. λ and κ are the dimensionless coefficients parametrizing the interactions among the Higgs fields, the same as in the $\mathbb{Z}_3$ NMSSM. The bilinear mass parameters μ and μ' and the singlet tadpole parameter ξ describe the $\mathbb{Z}_3$-symmetry violating effects. They are advantageous to solve the tadpole problem [54,74] and the cosmological domain-wall problem of the $\mathbb{Z}_3$ NMSSM [75–77]. Noting that one of these parameters can be eliminated by shifting the $\hat{S}$ field and redefining the other parameters [78], we set ξ to be zero without losing the generality of this study. In this case, the bilinear parameters could stem from an underlying discrete R symmetry, Z_4^R or Z_8^R, after the SUSY breaking and might be naturally at the electroweak scale [75,78–81]. They can significantly change the Higgs and DM physics of the $\mathbb{Z}_3$ NMSSM, which is the focus of this study.

The soft SUSY-breaking Lagrangian for the Higgs fields in the GNMSSM is given by

$$-\mathcal{L}_{\mathrm{soft}} = \left[\lambda A_\lambda S H_u\cdot H_d + \frac{1}{3}\kappa A_\kappa S^3 + m_3^2 H_u\cdot H_d + \frac{1}{2}m_S'^2 S^2 + \mathrm{H.c.}\right] + m_{H_u}^2|H_u|^2 + m_{H_d}^2|H_d|^2 + m_S^2|S|^2, \tag{2.2}$$

where H_u, H_d, and S denote the scalar components of the Higgs superfields, and $m^2_{H_u}$, $m^2_{H_d}$, and m^2_S are their soft-breaking masses. After these parameters are fixed by solving the conditional equations to minimize the scalar potential and expressed in terms of the vacuum expectation values of the Higgs fields, $\langle H^0_u\rangle = v_u/\sqrt{2}$, $\langle H^0_d\rangle = v_d/\sqrt{2}$, and $\langle S\rangle = v_s/\sqrt{2}$ with $v = \sqrt{v_u^2 + v_d^2} \simeq 246$ GeV, the Higgs sector is described by the following ten free parameters: $\tan\beta \equiv v_u/v_d$, v_s, the Yukawa couplings λ and κ, the soft-breaking trilinear coefficients A_λ and A_κ, the bilinear mass parameters μ and μ', and their soft-breaking parameters m_3^2 and $m_S'^2$.

In revealing the characteristics of Higgs physics, it is customary to introduce the field combinations of $H_{\rm SM} \equiv \sin\beta {\rm Re}(H^0_u) + \cos\beta {\rm Re}(H^0_d)$, $H_{\rm NSM} \equiv \cos\beta {\rm Re}(H^0_u) - \sin\beta {\rm Re}(H^0_d)$, and $A_{\rm NSM} \equiv \cos\beta {\rm Im}(H^0_u) - \sin\beta {\rm Im}(H^0_d)$, where $H_{\rm SM}$ stands for the SM Higgs field, and $H_{\rm NSM}$ and $A_{\rm NSM}$ represent the extra doublet fields [73]. The elements of CP-even Higgs boson mass matrix $\mathcal{M}_S^2$ in the bases $(H_{\rm NSM}, H_{\rm SM}, {\rm Re}[S])$ are written as [54,82]

$$\begin{aligned}
\mathcal{M}^2_{S,11} &= \frac{\lambda v_s(\sqrt{2}A_\lambda + \kappa v_s + \sqrt{2}\mu') + 2m_3^2}{\sin 2\beta} + \frac{1}{2}(2m_Z^2 - \lambda^2 v^2)\sin^2 2\beta,\\
\mathcal{M}^2_{S,12} &= -\frac{1}{4}(2m_Z^2 - \lambda^2 v^2)\sin 4\beta, \qquad \mathcal{M}^2_{S,13} = -\frac{\lambda v}{\sqrt{2}}(A_\lambda + \sqrt{2}\kappa v_s + \mu')\cos 2\beta,\\
\mathcal{M}^2_{S,22} &= m_Z^2\cos^2 2\beta + \frac{1}{2}\lambda^2 v^2 \sin^2 2\beta,\\
\mathcal{M}^2_{S,23} &= \frac{\lambda v}{\sqrt{2}}\left[(\sqrt{2}\lambda v_s + 2\mu) - (A_\lambda + \sqrt{2}\kappa v_s + \mu')\sin 2\beta\right],\\
\mathcal{M}^2_{S,33} &= \frac{(A_\lambda + \mu')\sin 2\beta}{2\sqrt{2}v_s}\lambda v^2 + \frac{\kappa v_s}{\sqrt{2}}(A_\kappa + 2\sqrt{2}\kappa v_s + 3\mu') - \frac{\mu}{\sqrt{2}v_s}\lambda v^2,
\end{aligned} \tag{2.3}$$

and those for CP-odd Higgs fields in the bases $(A_{\rm NSM}, {\rm Im}(S))$ take the following forms:

$$\begin{aligned}
\mathcal{M}^2_{P,11} &= \frac{\lambda v_s(\sqrt{2}A_\lambda + \kappa v_s + \sqrt{2}\mu') + 2m_3^2}{\sin 2\beta}, \qquad \mathcal{M}^2_{P,12} = \frac{\lambda v}{\sqrt{2}}(A_\lambda - \sqrt{2}\kappa v_s - \mu'),\\
\mathcal{M}^2_{P,22} &= \frac{(A_\lambda + 2\sqrt{2}\kappa v_s + \mu')\sin 2\beta}{2\sqrt{2}v_s}\lambda v^2 - \frac{\kappa v_s}{\sqrt{2}}(3A_\kappa + \mu') - \frac{\mu}{\sqrt{2}v_s}\lambda v^2 - 2m_S'^2.
\end{aligned} \tag{2.4}$$

After diagonalizing $\mathcal{M}_S^2$ and $\mathcal{M}_P^2$ with unitary matrices V and U, respectively, three CP-even and two CP-odd Higgs mass eigenstates, denoted as $h_i = \{h, H, h_{\rm s}\}$ and $a_j = \{A_H, A_s\}$, respectively, are obtained:

$$\begin{aligned}
h_i &= V^{\rm NSM}_{h_i} H_{\rm NSM} + V^{\rm SM}_{h_i} H_{\rm SM} + V^{\rm S}_{h_i}{\rm Re}[S],\\
a_j &= U^{\rm NSM}_{a_j} A_{\rm NSM} + U^{\rm S}_{a_j}{\rm Im}[S],
\end{aligned} \tag{2.5}$$

where h means the SM-like Higgs boson discovered at the LHC, H and A_H represent heavy doublet-dominated Higgs bosons, and h_s and A_s are singlet-dominated scalars. The model also predicts a pair of charged Higgs, $H^\pm = \cos\beta H_u^\pm + \sin\beta H_d^\pm$, and its squared mass is

$$m^2_{H_\pm} = \frac{\lambda v_s(\sqrt{2}A_\lambda + \kappa v_s + \sqrt{2}\mu') + 2m_3^2}{\sin 2\beta} + m_W^2 - \frac{1}{2}\lambda^2 v^2. \tag{2.6}$$

The Higgs sector of the GNMSSM has the following features:

(1) The experimental data have restricted the $H_{\rm NSM}$ and ${\rm Re}[S]$ components in h to be less than 10% [83,84], i.e., $\sqrt{(V^{\rm NSM}_h)^2 + (V^{\rm S}_h)^2} \lesssim 0.1$ and $|V^{\rm SM}_h| \sim 1$. In the limit of $\tan\beta \gg 1$, h is mainly composed of the field ${\rm Re}[H^0_u]$, and H has the most significant component from ${\rm Re}[H^0_d]$.

(2) The CP-even doublet scalar H almost degenerates with the CP-odd scalar A_H and the charged Higgs bosons $H^\pm$ in mass. The LHC searches for extra Higgs bosons combined with the indirect constraints from B physics prefer these bosons to be massive, e.g., $m_H \gtrsim 0.5$ TeV [10,85].

(3) Current collider data allow the singlet-dominated scalars to be moderately light and contain sizable doublet components [66], which is the starting point of this study.

The neutralino sector in the GNMSSM consists of the bino field $\tilde{B}$, the wino field $\tilde{W}$, the higgsino fields $\tilde{H}_d^0$ and $\tilde{H}_u^0$, and the singlino field $\tilde{S}$. In the bases $\psi \equiv (\tilde{B}, \tilde{W}, \tilde{H}_d^0, \tilde{H}_u^0, \tilde{S})$, the symmetric neutralino mass matrix takes the following form [54]:

$$\mathcal{M} = \begin{pmatrix} M_1 & 0 & -m_Z \sin\theta_W \cos\beta & m_Z \sin\theta_W \sin\beta & 0 \\ & M_2 & m_Z \cos\theta_W \cos\beta & -m_Z \cos\theta_W \sin\beta & 0 \\ & & 0 & -\mu_{\rm tot} & -\frac{1}{\sqrt{2}}\lambda v \sin\beta \\ & & & 0 & -\frac{1}{\sqrt{2}}\lambda v \cos\beta \\ & & & & m_N \end{pmatrix}, \tag{2.7}$$

where θ_W is the weak mixing angle, and M_1 and M_2 are the soft-breaking masses of the bino and wino fields, respectively. The higgsino mass $\mu_{\rm tot}$ and the singlino mass m_N are given by $\mu_{\rm tot} \equiv \lambda v_s/\sqrt{2} + \mu$ and $m_N \equiv \sqrt{2}\kappa v_s + \mu'$. Diagonalizing $\mathcal{M}$ by a rotation matrix N then yields five mass eigenstates:

$$\tilde{\chi}_i^0 = N_{i1}\psi_1^0 + N_{i2}\psi_2^0 + N_{i3}\psi_3^0 + N_{i4}\psi_4^0 + N_{i5}\psi_5^0, \tag{2.8}$$

where $\tilde{\chi}_i^0$ ($i = 1, 2, 3, 4, 5$) are labeled in a mass-ascending order, and the matrix element N_{ij} parametrizes the component of the field ψ_j^0 in $\tilde{\chi}_i^0$. The lightest neutralino $\tilde{\chi}_1^0$ usually acts as a viable DM candidate, and it may be bino dominated ($\tilde{B}$ dominated) or singlino dominated ($\tilde{S}$ dominated) to acquire the measured DM relic density [67]. One distinct feature of the GNMSSM is that the singlet-dominated scalars may play crucial roles in DM physics if $\tilde{\chi}_1^0$ is the $\tilde{S}$ dominated [64,67]. Specifically, owing to the singlet-doublet coupling and the self-interaction term in the superpotential, these scalars may mediate the DM annihilation and the DM-nucleon scattering. They may also present themselves as the final state of the annihilation.

Notably, so far the physical implications of A_κ, μ, μ', m_3^2, and $m_S'^2$ are vague, which motivated us to replace them with the masses of the heavy doublet Higgs fields, the CP-even and -odd singlet Higgs fields, and the higgsino and singlino fields, denoted as $m_A \equiv \sqrt{\mathcal{M}_{P,11}^2}$, $m_B \equiv \sqrt{\mathcal{M}_{S,33}^2}$, $m_C \equiv \sqrt{\mathcal{M}_{P,22}^2}$, $\mu_{\rm tot}$, and m_N, respectively. With this new set of inputs, the following identities give A_κ, μ, μ', m_3^2, and $m_S'^2$:

$$\begin{aligned} \mu &= \mu_{\rm tot} - \frac{\lambda}{\sqrt{2}} v_s, \qquad \mu' = m_N - \sqrt{2}\kappa v_s, \qquad m_3^2 = \frac{m_A^2 \sin 2\beta}{2} - \lambda v_s \left(\frac{\kappa v_s}{2} + \frac{\mu'}{\sqrt{2}} + \frac{A_\lambda}{\sqrt{2}}\right), \\ \kappa A_\kappa &= \frac{\sqrt{2} m_B^2}{v_s} + \frac{\lambda \mu v^2}{v_s^2} - \frac{\lambda (A_\lambda + \mu') v^2 \sin 2\beta}{2 v_s^2} - 2\sqrt{2}\kappa^2 v_s - 3\kappa\mu', \\ m_S'^2 &= -\frac{1}{2}\left[m_C^2 + \frac{\lambda \mu v^2}{\sqrt{2} v_s} + \frac{\kappa v_s (3A_\kappa + \mu')}{\sqrt{2}} - \frac{\lambda (A_\lambda + 2\sqrt{2}\kappa v_s + \mu') v^2 \sin 2\beta}{2\sqrt{2} v_s}\right]. \end{aligned} \tag{2.9}$$

Equations (2.3), (2.4), and (2.6) are rewritten as

$$\begin{aligned} \mathcal{M}_{S,11}^2 &= m_A^2 + \frac{1}{2}(2m_Z^2 - \lambda^2 v^2)\sin^2 2\beta, \qquad \mathcal{M}_{S,12}^2 = -\frac{1}{4}(2m_Z^2 - \lambda^2 v^2)\sin 4\beta, \\ \mathcal{M}_{S,13}^2 &= -\frac{\lambda v}{\sqrt{2}}(A_\lambda + m_N)\cos 2\beta, \qquad \mathcal{M}_{S,22}^2 = m_Z^2 \cos^2 2\beta + \frac{1}{2}\lambda^2 v^2 \sin^2 2\beta, \\ \mathcal{M}_{S,23}^2 &= \frac{\lambda v}{\sqrt{2}}[2\mu_{\rm tot} - (A_\lambda + m_N)\sin 2\beta], \qquad \mathcal{M}_{S,33}^2 = m_B^2, \mathcal{M}_{P,11}^2 = m_A^2, \\ \mathcal{M}_{P,22}^2 &= m_C^2, \qquad \mathcal{M}_{P,12}^2 = \frac{\lambda v}{\sqrt{2}}(A_\lambda - m_N), \qquad m_{H_\pm}^2 = m_A^2 + m_W^2 - \frac{1}{2}\lambda^2 v^2. \end{aligned} \tag{2.10}$$

In the limit of $\lambda \to 0$, the singlet field will decouple from the doublet Higgs fields, and the field masses can be regarded as physical particle masses to a good approximation. Although this situation cannot be directly applied to this study, we

verified that adopting the new set of parameters as inputs could significantly boost the process of acquiring the solutions to the excesses compared with the old set of inputs.

B. Formula for the $\gamma\gamma$ and $b\bar{b}$ signals

This work assumes h_s to be responsible for the excesses. In the narrow width approximation, the diphoton signal strength normalized to its SM prediction is given by

$$\begin{aligned}\mu_{\gamma\gamma}|_{m_{h_s}=95.4\text{ GeV}} &= \frac{\sigma_{\rm SUSY}(pp\to h_s)}{\sigma_{\rm SM}(pp\to h_s)}\times\frac{\mathrm{Br}_{\rm SUSY}(h_s\to\gamma\gamma)}{\mathrm{Br}_{\rm SM}(h_s\to\gamma\gamma)}\\ &\simeq \frac{\sigma_{\rm SUSY,ggF}(pp\to h_s)}{\sigma_{\rm SM,ggF}(pp\to h_s)}\times\frac{\Gamma_{\rm SUSY}(h_s\to\gamma\gamma)}{\Gamma_{\rm SM}(h_s\to\gamma\gamma)}\times\frac{\Gamma^{\rm tot}_{\rm SM}}{\Gamma^{\rm tot}_{\rm SUSY}}\\ &\simeq \frac{\Gamma_{\rm SUSY}(h_s\to gg)}{\Gamma_{\rm SM}(h_s\to gg)}\times\frac{\Gamma_{\rm SUSY}(h_s\to\gamma\gamma)}{\Gamma_{\rm SM}(h_s\to\gamma\gamma)}\times\frac{1}{\mathrm{R}_{\rm Width}},\\ &\simeq |C_{h_sgg}|^2\times|C_{h_s\gamma\gamma}|^2\times\frac{1}{\mathrm{R}_{\rm Width}},\end{aligned}\tag{2.11}$$

where the mass of h_s is fixed at 95.4 GeV, the production rate $\sigma(pp\to h_s)$, the decay branching ratio $\mathrm{Br}(h_s\to\gamma\gamma)$, and the width Γ, all labeled with the subscript "SUSY," refer to the predictions of the GNMSSM, and those with the subscript "SM" are acquired by assuming h_s to have SM couplings. Since the gluon fusion (ggF) process is the primary contribution to the Higgs production [3,5], we take $\sigma_{\rm SUSY}(pp\to h_s)/\sigma_{\rm SM}(pp\to h_s)\simeq\sigma_{\rm SUSY,ggF}(pp\to h_s)/\sigma_{\rm SM,ggF}(pp\to h_s)\simeq\Gamma_{\rm SUSY}(h_s\to gg)/\Gamma_{\rm SM}(h_s\to gg)\simeq|C_{h_sgg}|^2$, where C_{h_sgg} is the ratio of the h_s-gluon-gluon coupling strengths, $C_{h_sgg}\equiv\mathcal{A}^{h_sgg}_{\rm SUSY}/\mathcal{A}^{h_sgg}_{\rm SM}$. The normalized coupling strength of h_s to photons, $C_{h_s\gamma\gamma}$, is similarly defined. Besides, the width $\Gamma^{\rm tot}_{\rm SUSY}$ and the ratio $\mathrm{R}_{\rm Width}\equiv\Gamma^{\rm tot}_{\rm SUSY}/\Gamma^{\rm tot}_{\rm SM}$ are acquired by

$$\begin{aligned}\Gamma^{\rm tot}_{\rm SUSY} &= \Gamma_{\rm SUSY}(h_s\to b\bar{b})+\Gamma_{\rm SUSY}(h_s\to\tau\bar{\tau})+\Gamma_{\rm SUSY}(h_s\to c\bar{c})+\Gamma_{\rm SUSY}(h_s\to gg)+\cdots\\ &= |C_{h_sb\bar{b}}|^2\times\Gamma_{\rm SM}(h_s\to b\bar{b})+|C_{h_s\tau\bar{\tau}}|^2\times\Gamma_{\rm SM}(h_s\to\tau\bar{\tau})+|C_{h_sc\bar{c}}|^2\times\Gamma_{\rm SM}(h_s\to c\bar{c})\\ &\quad+|C_{h_sgg}|^2\times\Gamma_{\rm SM}(h_s\to gg)+\cdots,\\ \mathrm{R}_{\rm Width} &= |C_{h_sb\bar{b}}|^2\times\mathrm{Br}_{\rm SM}(h_s\to b\bar{b})+|C_{h_s\tau\bar{\tau}}|^2\times\mathrm{Br}_{\rm SM}(h_s\to\tau\bar{\tau})+|C_{h_sc\bar{c}}|^2\times\mathrm{Br}_{\rm SM}(h_s\to c\bar{c})\\ &\quad+|C_{h_sgg}|^2\times\mathrm{Br}_{\rm SM}(h_s\to gg)+\cdots,\\ &\simeq 0.801\times|C_{h_sb\bar{b}}|^2+0.083\times|C_{h_s\tau\bar{\tau}}|^2+0.041\times|C_{h_sc\bar{c}}|^2+0.067\times|C_{h_sgg}|^2,\end{aligned}\tag{2.12}$$

respectively, where $C_{h_sf\bar{f}}$ ($f=b,\tau,c$) are the normalized couplings of h_s to the fermion pair $f\bar{f}$ defined by $C_{h_sf\bar{f}}\equiv\mathcal{A}^{h_sf\bar{f}}_{\rm SUSY}/\mathcal{A}^{h_sf\bar{f}}_{\rm SM}$, and the branching ratios in the SM were obtained by the LHC Higgs Cross Section Working Group, which included all known higher-order QCD corrections [86].

Similarly, the normalized signal strength of the $b\bar{b}$ excess follows from

$$\begin{aligned}\mu_{b\bar{b}}|_{m_{h_s}=95.4\text{ GeV}} &= \frac{\sigma_{\rm SUSY}(e^+e^-\to Zh_s)}{\sigma_{\rm SM}(e^+e^-\to Zh_s)}\times\frac{\mathrm{Br}_{\rm SUSY}(h_s\to b\bar{b})}{\mathrm{Br}_{\rm SM}(h_s\to b\bar{b})}\\ &= |C_{h_sVV}|^2\times|C_{h_sb\bar{b}}|^2\times\frac{1}{\mathrm{R}_{\rm Width}}.\end{aligned}\tag{2.13}$$

Note that the produced Higgs boson must be CP-even to explain the $b\bar{b}$ excess, since a CP-odd one does not couple to Z boson and thus gives no contributions. By contrast, the scalar may be either CP-even or CP-odd to account for the diphoton excess.

In the GNMSSM, $\mathcal{A}^{h_sgg}_{\rm SUSY}$ is contributed by the loops mediated by quarks and squarks [87]. The code SPheno-4.0.5 [88,89] calculates it by the following formula:

$$\begin{aligned}\mathcal{A}^{h_sgg}_{\rm SUSY} &= \sum_q\mathcal{A}^{h_sgg,q}_{\rm SUSY}+\sum_{\tilde{q}}\mathcal{A}^{h_sgg,\tilde{q}}_{\rm SUSY}\\ &= \sum_q C^{\rm tree}_{h_sq\bar{q}}\times\frac{m_q(Q)}{m_q(\text{pole})}\times\mathcal{A}^{h_sgg,q}_{\rm SM}+\sum_{\tilde{q}}\mathcal{A}^{h_sgg,\tilde{q}}_{\rm SUSY}\end{aligned}\tag{2.14}$$

where $\mathcal{A}^{h_sgg,q}_{\rm SUSY}$ and $\mathcal{A}^{h_sgg,\tilde{q}}_{\rm SUSY}$ represent the quark and squark contributions, respectively, to the h_sgg coupling in the

GNMSSM [90], $\mathcal{A}_{\rm SM}^{h_s gg,q}$ denotes the quark contribution in the SM with its one-loop expression given in Ref. [91], $C_{h_s q\bar{q}}^{\rm tree}$ is the tree-level prediction of $C_{h_s q\bar{q}}$, and $m_q(Q)$ and m_q(pole) are the quark running mass at the scale $Q \simeq m_{h_s}$ and the pole mass, respectively. Note that the code has incorporated the higher-order QCD corrections to $\mathcal{A}_{\rm SM}^{h_s gg,q}$ by the formulas in Ref. [92,93]. $\mathcal{A}_{\rm SUSY}^{h_s\gamma\gamma}(Q)$ is similarly obtained, except that it receives additional contributions from the W boson, charged Higgs boson, and chargino-mediated loops [87]. We add that the supersymmetric contributions to $C_{h_s gg}$ and $C_{h_s\gamma\gamma}$ are not crucial in this study. Specifically, given the massiveness of the squarks, their contributions to the couplings are typically a few thousandths. The charginos' contribution to $C_{h_s\gamma\gamma}$ only reaches 1% in an optimum case since λ is minor [94], and the charged Higgs's contribution is at the level of 0.001%.

In this study, we acquired the normalized couplings of h_s to fermions, WW, and ZZ by their tree-level expressions.[3] After neglecting the difference of the running mass and the pole mass and the supersymmetric contributions, we had the following relations [54]:

$$\begin{aligned}
&C_{h_s t\bar{t}} = V_{h_s}^{\rm SM} + V_{h_s}^{\rm NSM}\cot\beta \simeq V_{h_s}^{\rm SM},\\
&C_{h_s b\bar{b}} = V_{h_s}^{\rm SM} - V_{h_s}^{\rm NSM}\tan\beta, \qquad C_{h_s VV} = V_{h_s}^{\rm SM},\\
&C_{h_s c\bar{c}} = C_{h_s t\bar{t}}, \qquad C_{h_s\tau\bar{\tau}} = C_{h_s b\bar{b}},\\
&C_{h_s gg} \simeq C_{h_s t\bar{t}}, \qquad C_{h_s\gamma\gamma} \simeq V_{h_s}^{\rm SM},
\end{aligned} \tag{2.15}$$

where the rotation matrix elements V_j^i are defined in Eq. (2.5). We also concluded $V_{h_s}^{\rm SM} \simeq 0.36$ and $(V_{h_s}^{\rm SM} - V_{h_s}^{\rm NSM}\tan\beta) \simeq 0.70 \times V_{h_s}^{\rm SM} \simeq 0.25$ (or equivalently, $V_{h_s}^{\rm NSM}\tan\beta \simeq 0.11$) to acquire the central values of $\mu_{\gamma\gamma}$ and $\mu_{b\bar{b}}$ and the preferred branching ratios to be ${\rm Br}_{\rm SUSY}(h_s\to\gamma\gamma) \simeq 1.86\times{\rm Br}_{\rm SM}(h_s\to\gamma\gamma) \simeq 2.58\times10^{-3}$ and ${\rm Br}_{\rm SUSY}(h_s\to b\bar{b}) \simeq 0.90\times{\rm Br}_{\rm SM}(h_s\to b\bar{b}) \simeq 72.6\%$. Alternatively, if we obtained $C_{h_s gg}$ and $C_{h_s\gamma\gamma}$ by the exact formulas, as we always did in this study, these couplings might deviate from $C_{h_s t\bar{t}}$ by 4% and 11%, respectively. In this case, we found the central values of $\mu_{\gamma\gamma}$ and $\mu_{b\bar{b}}$ corresponded to $V_{h_s}^{\rm SM} \simeq 0.35$, $(V_{h_s}^{\rm SM} - V_{h_s}^{\rm NSM}\tan\beta) \simeq 0.81 \times V_{h_s}^{\rm SM} \simeq 0.28$, or equivalently, $V_{h_s}^{\rm NSM}\tan\beta \simeq 0.07$, ${\rm Br}_{\rm SUSY}(h_s\to\gamma\gamma) \simeq 1.77\times{\rm Br}_{\rm SM}(h_s\to\gamma\gamma) \simeq 2.5\times10^{-3}$, and ${\rm Br}_{\rm SUSY}(h_s\to b\bar{b}) \simeq 0.95\times{\rm Br}_{\rm SM}(h_s\to b\bar{b}) \simeq 76.1\%$. These results reveal that explaining the excesses requires an appropriate $C_{h_s t\bar{t}}$ and simultaneously a relatively suppressed $C_{h_s b\bar{b}}$, which are mainly decided by the Higgs mixings V_i^j. Particularly, the small deviations of $C_{h_s gg}$ and $C_{h_s\gamma\gamma}$ from $C_{h_s t\bar{t}}$ can significantly reduce $V_{h_s}^{\rm NSM}\tan\beta$ needed to predict the central values of the excesses, but hardly change $V_{h_s}^{\rm SM}$. In addition, the approximations also indicate that any reduction of $V_{h_s}^{\rm NSM}\tan\beta$ can enhance $C_{h_s b\bar{b}}$, leading to the increase of $\mu_{b\bar{b}}$ and the decrease of $\mu_{\gamma\gamma}$ if $C_{h_s gg}$, $C_{h_s\gamma\gamma}$, and $C_{h_s VV}$ are fixed.[4] It explains the prediction of $\mu_{b\bar{b}} > 0.117$ for $\mu_{\gamma\gamma} = 0.24$, frequently encountered in this study and shown in Fig. 11.

Furthermore, we point out that explaining the diphoton and $b\bar{b}$ excesses nontrivially restricts the parameters in the Higgs sector. Specifically, after neglecting the renormalization group running of the input parameters and the radiative corrections to $\mathcal{M}_S^2$ in Eq. (2.10), one can express the eigenstate equations of h_s as follows:

$$\sum_{j={\rm NSM,SM,S}} [\mathcal{M}_S^2]_j^i V_{h_s}^j = m_{h_s}^2 V_{h_s}^i. \tag{2.16}$$

Noting $m_{h_s}, m_h \ll m_A$, implying that the mixings of $H_{\rm NSM}$ with $H_{\rm SM}$ and ${\rm Re}[S]$ are small, we acquire the following approximations:

$$\begin{aligned}
V_{h_s}^{\rm NSM} &\simeq -\frac{V_{h_s}^S}{\sqrt{2}}\times\frac{\lambda(A_\lambda + m_N)v}{m_A^2},\\
\lambda\mu_{\rm tot} &\simeq \frac{V_{h_s}^{\rm SM}V_{h_s}^S}{\sqrt{2}}\times\frac{m_{h_s}^2 - m_h^2}{v},\\
m_B^2 &\simeq m_{h_s}^2|V_{h_s}^S|^2 + m_h^2|V_{h_s}^{\rm SM}|^2,\\
\mathcal{M}_{S,22}^2 &\simeq m_h^2|V_{h_s}^S|^2 + m_{h_s}^2|V_{h_s}^{\rm SM}|^2,
\end{aligned} \tag{2.17}$$

in the large $\tan\beta$ limit. These expressions indicate that the observed excesses have restricted m_B and $\mathcal{M}_{S,22}$ within narrow ranges. They also suggest

$$\lambda \simeq 0.06\times\left(\frac{V_{h_s}^{\rm SM}}{0.35}\right)\times\left(\frac{\mu_{\rm tot}}{100\ {\rm Gev}}\right)^{-1}, \tag{2.18}$$

and

$$\lambda \gtrsim 0.014\times\left(\frac{\tan\beta}{30}\right)^{-1}\times\left(\frac{A_\lambda + m_N}{1\ {\rm TeV}}\right)^{-1}\times\left(\frac{m_A}{1\ {\rm TeV}}\right)^2, \tag{2.19}$$

to predict $V_{h_s}^{\rm NSM}\tan\beta \gtrsim 0.07$. Given that the LHC searches for electroweakinos have established $\mu_{\rm tot} \gtrsim 200$ GeV [96], it can be inferred that elucidating the observed excesses favors $\lambda \lesssim 0.03$. Consequently for $m_A = 1$ TeV, one can deduce $\tan\beta/30\times(A_\lambda + m_N) \gtrsim 2$ TeV.

[3]The potentially large SUSY-QCD and SUSY-electroweak corrections to the bottom quark Yukawa coupling are minor in this study since gluino and squarks are very massive [95].

[4]This assumption is plausible since $C_{h_s gg}$ and $C_{h_s\gamma\gamma}$ are insensitive to $C_{h_s b\bar{b}}$, and $C_{h_s VV}$ is independent of $C_{h_s b\bar{b}}$.

TABLE I. The parameter space explored in this study, assuming all the inputs were flatly distributed in prior since they have clear physical meanings. Considering that the soft trilinear coefficients for the third-generation squarks, A_t and A_b, could significantly affect the SM-like Higgs boson mass by radiative corrections, we took $A_t = A_b$ and varied them. The unmentioned dimensional SUSY parameters were not crucial to this study, so we fixed $M_3 = 3$ TeV, $m_C = 800$ GeV, and a shared value of 2 TeV for the others to be consistent with the LHC search for new physics. We defined all these parameters at the renormalization scale $Q_{inp} = 1$ TeV and *acquired the space by several trial scans over much broader parameter spaces*.

Parameter	Prior	Range	Parameter	Prior	Range
λ	Flat	0–0.03	κ	Flat	−0.2–0.2
$\tan\beta$	Flat	5–60	v_s/TeV	Flat	0.1–1.0
A_t/TeV	Flat	1.0–3.0	A_λ/TeV	Flat	0–2.0
m_A/TeV	Flat	0.6–2.0	m_B/GeV	Flat	90–120
$\mu_{\rm tot}$/TeV	Flat	0.4–1.0	m_N/TeV	Flat	−1.0–1.0
M_1/TeV	Flat	−1.0– − 0.2	M_2/TeV	Flat	0.3–1.0

III. EXPLANATION OF THE EXCESSES

This section introduces our sampling strategy and explains the excesses based on numerical results. We utilized the package SARAH-4.14.3 [97–100] to build the model routines of the GNMSSM and the codes SPheno-4.0.5 [88,89] and FlavorKit [101] to generate particle spectrum and compute low energy flavor observables, respectively. We calculated the DM physics observables with the package MicrOMEGAs-5.0.4 [102–111]. We analyzed the acquired samples using the posterior probability density function (PDF) in Bayesian inference and the profile likelihood (PL) in Frequentist statistics [112].

A. Research strategy

We performed a sophisticated scan over the parameter space in Table I, using the MultiNest algorithm with $nlive = 16000$ [113].[5] We constructed the following likelihood function to guide the scan[6]:

$$\begin{aligned}\mathcal{L} &\equiv \mathcal{L}_{\gamma\gamma+b\bar{b}} \times \mathcal{L}_{\rm Res} = \exp\left[-\frac{\chi^2_{\gamma\gamma+b\bar{b}}}{2}\right] \times \mathcal{L}_{\rm Res} \\ &= \exp\left\{-\frac{1}{2}\left[\left(\frac{\mu_{\gamma\gamma}-0.24}{0.08}\right)^2 + \left(\frac{\mu_{b\bar{b}}-0.117}{0.057}\right)^2\right]\right\}_{m_{h_s}\simeq 95\ \rm GeV} \times \mathcal{L}_{\rm Res}, \end{aligned} \tag{3.1}$$

where $\mathcal{L}_{\rm Res}$ represented the restrictions from pertinent experiments on the theory: $\mathcal{L}_{\rm Res} = 1$ by our definition if the limitations were satisfied, and otherwise, $\mathcal{L}_{\rm Res} = \exp[-100]$. These restrictions included

(1) A proper h_s mass range to explain the excesses: 94.4 GeV $\le m_{h_s} \le$ 96.4 GeV, where we assumed 1 GeV theoretical and experimental uncertainties in determining m_{h_s}.
(2) Higgs data fit. Given that h corresponded to the LHC-discovered Higgs boson, its properties should be consistent with the Higgs measurements by the ATLAS and CMS Collaborations at the 95% confidence level. A p value larger than 0.05 was essential, which was tested by the code HiggsSignal-2.3.2 [116–119].
(3) Direct searches for extra Higgs bosons at LEP, Tevatron, and LHC. This requirement was implemented by the code HIGGSBOUNDS-5.10.2 [120–124].
(4) Pertinent DM relic density, $0.096 \le \Omega h^2 \le 0.144$. We took the central value of $\Omega h^2 = 0.120$ from the Planck-2018 data [125] and assumed theoretical uncertainties of 20% in the density calculation.

[5]*Nlive* in the MultiNest method signifies the number of active or live points determining the isolikelihood contour in each iteration [113,114]. The larger it is, the more detailed the scan process will be in surveying the parameter space.

[6]In deriving the likelihood function, we made the assumption of abundant production of the diphoton and $b\bar{b}$ events at colliders, which was unrealistic. Additionally, we overestimated the impact of the restrictions in excluding SUSY parameter space. As a result, the posterior PDF and PL depicted in Figs. 1, 2, 6, and 7 lack robust statistical significance; however, they do provide insights into the underlying physics behind the excesses. It is worth noting that a more realistic approach to formulating the likelihood function was introduced in Ref. [115] when globally fitting grand unified theory scale SUSY models to experimental observations.

(5) DM direct detection bounds from the LZ experiments on both the SI DM-nucleon scattering cross section, $\sigma_p^{\rm SI}$, and the SD one, $\sigma_n^{\rm SD}$ [55]. The DM indirect searches from the observation of dwarf galaxies by the Fermi-LAT Collaboration were not included since they had no restrictions on the GNMSSM when $|m_{\tilde{\chi}_1^0}| \gtrsim 100$ GeV [126].

(6) B-physics observables. The branching ratios of $B_s \to \mu^+\mu^-$ and $B \to X_s\gamma$ should be consistent with their experimental measurements at the 2σ level [127].

(7) Vacuum stability. The vacuum state of the Higgs potential should be either stable or long lived. This condition was tested by the code VEVACIOUS [128].

In this study, we were particularly interested in the samples that could explain the diphoton and $b\bar{b}$ excesses at the 2σ level and be consistent with all the restrictions. We decided whether they passed the limitations from the LHC search for the electroweakinos by the program SModelS– 2.1.1, which encoded various event-selection efficiencies by the topologies of SUSY signals [129]. Moreover, noting that the exclusion capability of this program on the samples was limited by its database and strict working prerequisites, we further surveyed some cases by simulating the analyses listed in Tables 1 of Ref. [70] and the research in Ref. [130],[7] adopting the strategy of Ref. [70]. We concluded that the LHC restriction had no impact on the results. We will explain this phenomenon later.

B. Numerical results

We acquired about 64000 samples that were consistent with the experimental restrictions. Analyzing the properties of the samples indicated that the DM might be $\tilde{B}$ dominated or $\tilde{S}$ dominated if one attempted to explain the excesses at the 2σ level, and they contributed to the total Bayesian evidence by 47% and 53%, respectively. In the following, we studied these two types of samples separately. We began with the popular $\tilde{B}$-dominated DM case, but we would show that the $\tilde{S}$-dominated DM case was superior to it in predicting a smaller $\chi^2_{\gamma\gamma+b\bar{b}}$ for the best point.

1. Bino-dominated DM case

We first studied the distributions of various theoretical parameters, including the one-dimensional PL and posterior PDF[8] of λ, κ, $\tan\beta$, v_s, A_t, and A_λ shown in Fig. 1; those of m_A, m_B, $\mu_{\rm tot}$, m_N, M_1, and M_2 in Fig. 2; and the scattering plots of the samples projected onto $M_2 - |m_{\tilde{\chi}_1^0}|$ and $\mu_{\rm tot} - |m_{\tilde{\chi}_1^0}|$ planes, respectively, in Fig. 3. The PL distributions indicate that the GNMSSM can explain the diphoton and $b\bar{b}$ excesses at the 2σ level in broad parameter space except that m_B and λ are restricted within narrow ranges. As noted in the approximations in Eqs. (2.17) and (2.18), the underlying reasons are as follows:

(1) Since the signal rates of the excesses have determined $V^{\rm S}_{h_s}$ and $V^{\rm SM}_{h_s}$, m_B is fixed by the relation $m_B^2 \simeq m_{h_s}^2|V^S_{h_s}|^2 + m_h^2|V^{\rm SM}_{h_s}|^2$, leading to 90 GeV$\lesssim m_B \lesssim$ 118 GeV;

(2) Barring no fine tunings, only the case characterized by a small λ and a sufficiently large $\mu_{\rm tot}$ can predict an appropriate $V^{\rm SM}_{h_s}$ to explain the excesses and simultaneously coincide with the results of the DM direct detection experiments and the LHC search for electroweakinos. We will discuss the LHC constraints later.

We emphasize that this small λ significantly suppresses $V^{\rm NSM}_{h_s}$. Consequently a sufficiently large $(A_\lambda + m_N)$ must be present to enhance $V^{\rm NSM}_{h_s}$, trying to satisfy the condition of $V^{\rm NSM}_{h_s}\tan\beta \simeq 0.10$ needed to acquire the central values of the excesses. This feature explains why the PL of A_λ monotonously increases as A_λ becomes large. Besides, m_A is restricted from about 1 TeV to 2 TeV, where the lower bound mainly originates from the LHC searches for extra Higgs bosons and B physics, and the upper bound

[7]ATLAS searched the electroweakino productions by fully hadronic final states [130], acquiring the hitherto tightest bounds on electroweakino masses. We encoded this analysis into package CheckMATE-2.0.26 [131–133] and validated our implementation in a manner similar to that described in Ref. [134].

[8]The frequentist PL is the most significant likelihood value in a specific parameter space [112]. Given a set of input parameters $\Theta \equiv (\Theta_1, \Theta_2, \cdots)$, one can acquire the one-dimensional PL by changing the other parameters to maximize the likelihood function, i.e.,

$$\mathcal{L}(\Theta_A) = \max_{\Theta_1,\ldots,\Theta_{A-1},\Theta_{A+1},\cdots} \mathcal{L}(\Theta).$$

The PL reflects the preference of a theory on the parameter space. For a given point Θ_A, it represents the capability of the point in the theory to account for experimental data. By contrast, the one-dimensional posterior PDF is obtained by integrating the posterior PDF from the Bayesian theorem, $P(\Theta)$, over the rest of the model inputs:

$$P(\Theta_A) = \int P(\Theta) d\Theta_1 d\Theta_2 \cdots d\Theta_{A-1} d\Theta_{A+1} \cdots\cdots.$$

It reflects the preference for the samples acquired in the scan. We emphasize that these definitions can be extended to high-dimensional distributions without changing their meanings. We also emphasize that these statistical measures depend on the studied parameter space, and the posterior PDF also depends on the prior distributions of the input parameters. The intrinsic physics of the considered theory determine all these quantities.

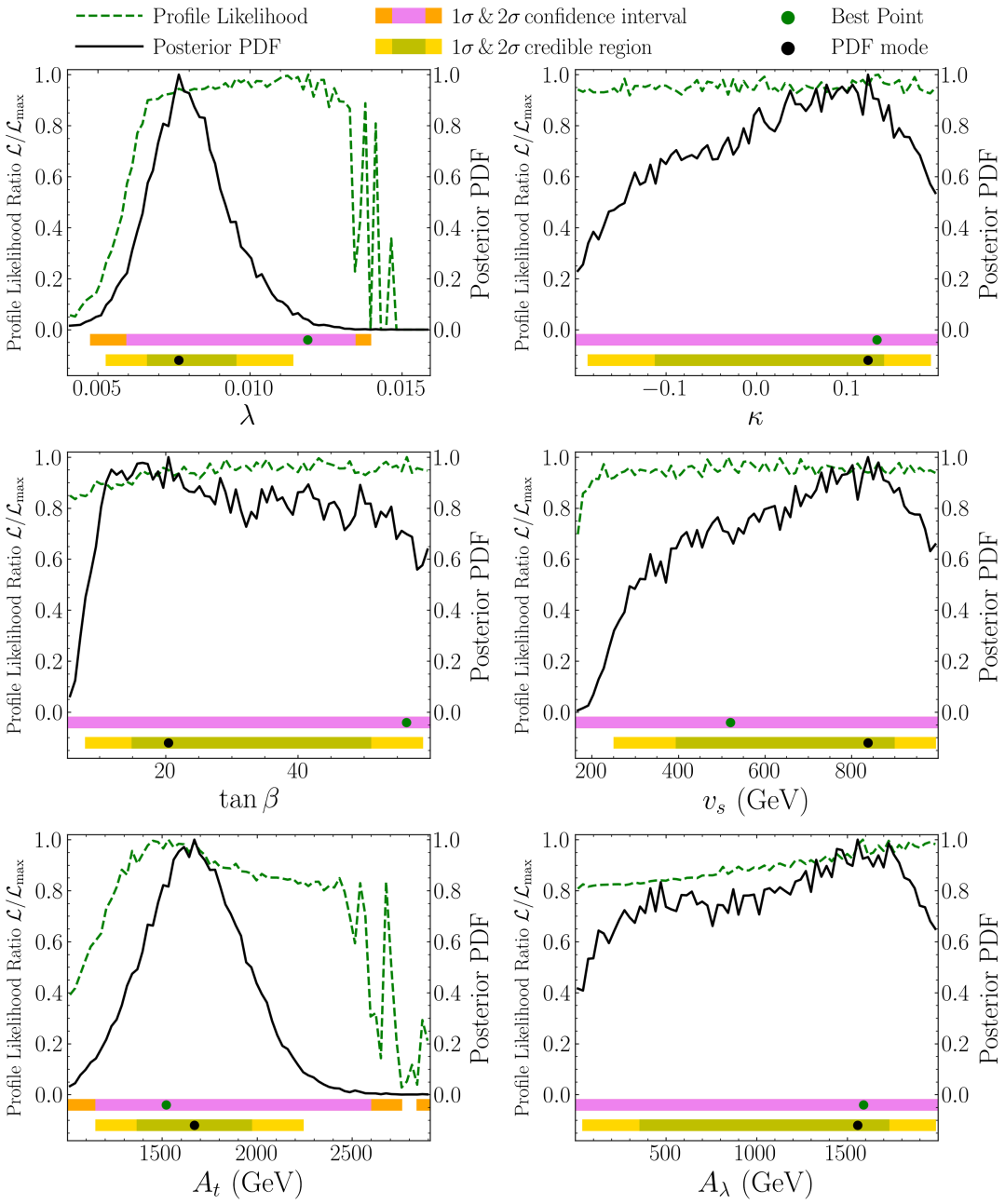

FIG. 1. One-dimensional profile likelihoods (dashed line) and posterior probability density functions (solid line) of the input parameters λ, κ, $\tan\beta$, v_s, A_t, and A_λ for the $\tilde{B}$-dominated DM case. The violet and orange bands show the 1σ and 2σ confidence intervals, respectively, and the green dot marks the best point corresponding to $\chi^2_{\gamma\gamma+b\bar{b}} = 0.27$. The yellow and golden bands denote the 1σ and 2σ credible regions, and the black dot denotes the mode of the posterior probability density function. All these statistical measures have been briefly introduced in Ref. [112]. Since we focus on the regions where both the profile likelihoods and the posterior distributions are large, the plotted ranges of the inputs are usually narrower than those listed in Table I.

arises from the boundary of the explored parameter space in Table I.

The posterior PDFs and the scattering plots reveal the following physics:

(1) The DM physics shown in Fig. 3 prefers relatively small $|M_1|$ and M_2, $|M_N| > |M_1|$, and simultaneously a large $\mu_{\rm tot}$. It also prefers a negative M_1 to suppress the SI DM-nucleon scattering by canceling different contributions [65]. Furthermore, since the $\tilde{B}$-dominated DM case is featured by a small λ and heavy higgsinos, the charginos' contribution to $C_{h_s\gamma\gamma}$ is always less than 1% [94].

(2) Although $V^{\rm NSM}_{h_s}$ depends on A_λ and m_A, the constraint $V^{\rm NSM}_{h_s}\tan\beta \gtrsim 10^{-2}$ favored for elucidating the

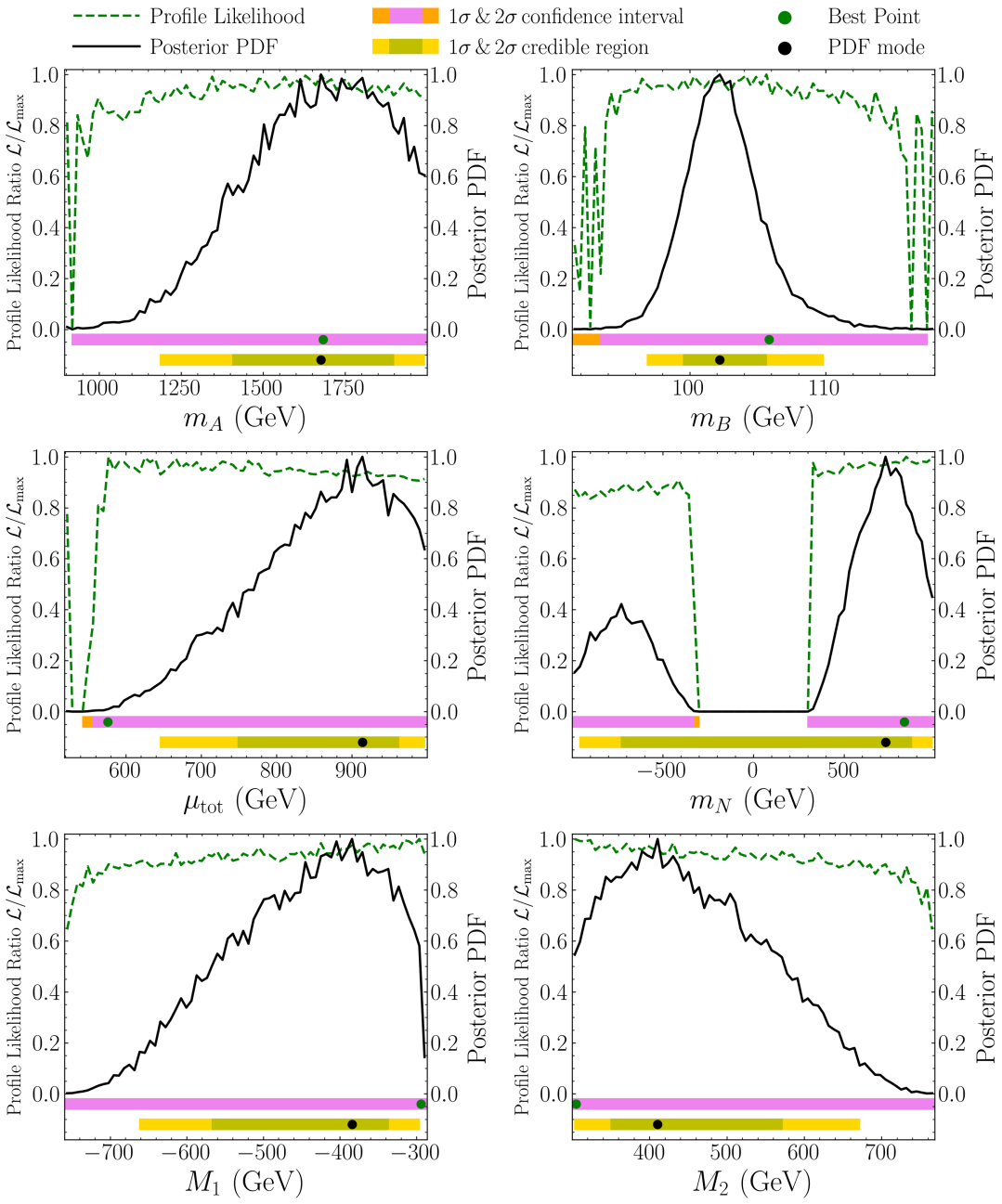

FIG. 2. Same as Fig. 1, but for the inputs m_A, m_B, $\mu_{\rm tot}$, m_N, M_1, and M_2.

observed excesses at the 2σ confidence level does not impose stringent limitations on the parameters A_λ, m_A, and $\tan\beta$. This condition can be readily satisfied through various avenues, particularly considering that the observed excess rates are not exceptionally high, and their theoretical predictions exhibit coherent relationships. One may understand this point by considering the extreme case where m_A in Eq. (2.17) is tremendously large or $(A_\lambda + m_N)$ vanishes, leading to $V_{h_s}^{\rm NSM} \simeq 0$, and consequently $C_{h_s b\bar{b}} \simeq C_{h_s t\bar{t}} \simeq C_{h_s gg} \simeq C_{h_s\gamma\gamma}$, and $\mu_{b\bar{b}} \simeq \mu_{\gamma\gamma}$. Then, the theoretical predictions of $\mu_{\gamma\gamma} = \mu_{b\bar{b}} = 0.117$ and $\mu_{b\bar{b}} = \mu_{\gamma\gamma} = 0.24$, easily achieved in the GNMSSM, correspond to $\chi^2_{\gamma\gamma+b\bar{b}} = 2.4$ and 4.7, respectively, implying that this case explains well the excesses.

In addition, it is noticeable that m_N tends to be of the same sign as A_λ to avoid a significant cancelation in contributing to $V_{h_s}^{\rm NSM}$. It is beneficial to acquire the central values of the excesses.

(3) The trilinear coefficient A_t significantly affects the SM-like Higgs boson mass m_h, the mixing $V_{h_s}^{\rm SM}$, and the $h_s gg$ and $h_s\gamma\gamma$ coupling strengths via $\tilde{t}$-mediated loops. Given that we have fixed the soft-breaking

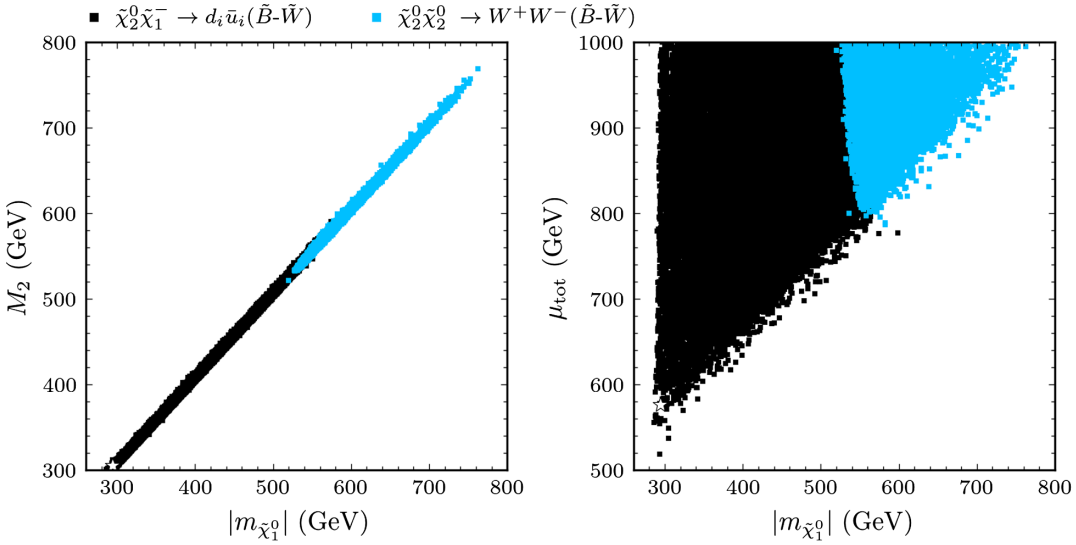

FIG. 3. Scattering plots of the samples predicting the $\tilde{B}$-dominated DM, projected onto $M_2 - |m_{\tilde{\chi}_1^0}|$ and $\mu_{\rm tot} - |m_{\tilde{\chi}_1^0}|$ planes, respectively. The left panel reveals that the DM achieved the measured relic abundance by coannihilating with the winolike electroweakinos. The largest contribution to the abundance comes from the channels $\tilde{\chi}_2^0\tilde{\chi}_1^- \to d_i\bar{u}_i$ ($i = 1, 2, 3$ denote the quark generations) for the black samples and the channel $\tilde{\chi}_2^0\tilde{\chi}_2^0 \to W^+W^-$ for the blue samples. The right panel indicates that the LZ results have set a lower bound of 520 GeV on $\mu_{\rm tot}$ for $|m_{\tilde{\chi}_1^0}| = 300$ GeV, given that the DM-nucleon scattering cross sections for the $\tilde{B}$-dominated DM are inversely proportional to $\mu_{\rm tot}^2$ [65]. This bound monotonously increases as the DM becomes heavier.

masses of the squarks at 2 TeV, A_t's around 1.7 TeV are preferred to make the theory accessible to explain the excesses.

(4) Equations (2.9) and (2.10) indicate that κ and v_s have no direct impacts on the observables involved in this study except that they enter the scalar potential of the singlet field and thus affect the electroweak symmetry breaking. Consequently, only the naturalness in realizing the symmetry breaking determines their posterior PDFs [135].

The scattering plots also reveal that the samples are hardly excluded by the LHC searches for electroweakinos. Specifically, the strategy of the LHC experiments in searching for SUSY relied on the mass splitting between the heavy sparticle produced at the LHC and the DM. It was categorized into the compressed spectrum case (Strategy I) and the significant mass splitting situation (Strategy II). Strategy I could test the bino-wino coannihilation samples by the wino-pair productions and Strategy II by the higgsino-pair productions. However, the former way was less efficient in this study because there were no restrictions on the coannihilation case if $m_{\tilde{\chi}_1^0} \gtrsim 220$ GeV, as shown in Fig. 16 of Ref. [96]. The latter way was also inefficient because both the higgsinos and the DM were heavy after comparing the right panel in Fig. 3 with Fig. 12 in Ref. [130]. Numerically speaking, we chose some points expected to have remarkable signals at the LHC and simulated the electroweakino productions with the package CheckMATE-2.0.26 [131–133]. We concluded that the acquired R values[9] were always less than 0.4. The fundamental reason for the weak restrictions is that explaining the excesses heavily relies on the Higgs mixings instead of sizable supersymmetric contributions to $C_{h_s gg}$ and $C_{h_s\gamma\gamma}$, which need the presence of light sparticles. The GNMSSM predicts broad parameter space to tune these mixings freely.

Next, we studied the properties of the Higgs bosons. In Fig. 4, we plotted the two-dimensional PL maps on the $|C_{h_sVV}| - |C_{h_s gg}|$, $|C_{h_s b\bar{b}}| - |C_{h_s t\bar{t}}|$, $|C_{h_s\gamma\gamma}| - |C_{h_s gg}|$, and $\mathrm{Br}(h_s \to b\bar{b}) - \mathrm{Br}(h_s \to \gamma\gamma)$ planes. This figure reveals $|C_{h_sVV}| \simeq |C_{h_s t\bar{t}}|$, that $|C_{h_s gg}|$ and $|C_{h_s\gamma\gamma}|$ are slightly larger than $|C_{h_s t\bar{t}}|$, and that explaining the excesses at the 2σ level prefers the region characterized by $0.20 \lesssim |C_{h_s t\bar{t}}| \lesssim 0.50$, $0.20 \lesssim |C_{h_s b\bar{b}}| \lesssim 0.50$ with the correlation of $|C_{h_s t\bar{t}}|/|C_{h_s b\bar{b}}| \simeq 1.1$, $1.85 \times 10^{-3} \lesssim \mathrm{Br}_{\rm SUSY}(h_s \to \gamma\gamma) \lesssim 2.40 \times 10^{-3}$, and $81\% \lesssim \mathrm{Br}_{\rm SUSY}(h_s \to b\bar{b}) \lesssim 83\%$. One can understand these features by the formulas of $\mu_{\gamma\gamma}$ and $\mu_{b\bar{b}}$ in Sec. II B. Besides, the best point predicts $|C_{h_s t\bar{t}}| \simeq 0.37$, $|C_{h_s b\bar{b}}| \simeq 0.34$, $\mathrm{Br}_{\rm SUSY}(h_s \to \gamma\gamma) \simeq 2.4 \times 10^{-3}$, and $\mathrm{Br}_{\rm SUSY}(h_s \to b\bar{b}) \simeq 81\%$, which significantly deviate from

[9]The R value is defined by $R \equiv \max\{S_i/S_{i,\rm obs}^{95}\}$, where S_i denotes the simulated event number of the ith signal region in the analyses listed in Tables 1 of Ref. [70] and the research in Ref. [130]. $S_{i,\rm obs}^{95}$ represents its 95% confidence level upper limit. $R < 1$ implies that the sample is consistent with the LHC search for SUSY.

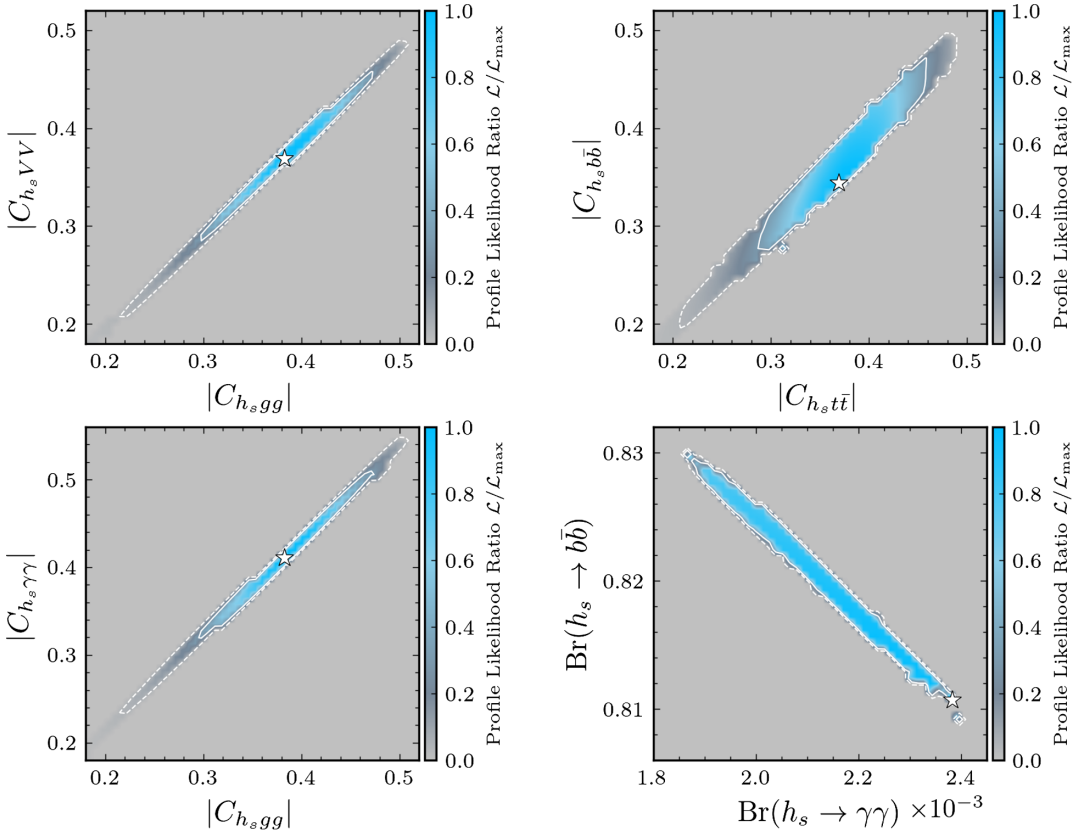

FIG. 4. Two-dimensional profile likelihood map of $\mathcal{L}_{\gamma\gamma+b\bar{b}}$ in Eq. (3.1), projected onto $|C_{h_s VV}| - |C_{h_s gg}|$, $|C_{h_s b\bar{b}}| - |C_{h_s t\bar{t}}|$, $|C_{h_s \gamma\gamma}| - |C_{h_s gg}|$, and $\mathrm{Br}(h_s \to \gamma\gamma) - \mathrm{Br}(h_s \to b\bar{b})$ planes, respectively. The best point is marked with a star symbol. Its $\chi^2_{\gamma\gamma+b\bar{b}}$ is equal to 0.27, and its other information is presented in Table II as the P1 point. The boundaries for 1σ and 2σ confidence intervals correspond to $\chi^2_{\gamma\gamma+b\bar{b}} = 2.3$ and $\chi^2_{\gamma\gamma+b\bar{b}} = 6.18$, respectively, which are labeled as solid and dashed lines.

the expectations in Sec. II B. The fundamental reason is it predicts $\mu_{\gamma\gamma} = 0.206$ and $\mu_{b\bar{b}} = 0.135$, sizeably away from their experimental central values. By contrast, we will show in Fig. 9 the best point for the $\tilde{S}$-dominated DM case, which predicts $\chi^2_{\gamma\gamma+b\bar{b}} \simeq 0$ and its other properties consistent with the expectations. We also studied the couplings of the SM-like Higgs boson in Fig. 5. This figure shows that the normalized couplings $|C_{hVV}|$, $|C_{ht\bar{t}}|$, $|C_{hb\bar{b}}|$, $|C_{hgg}|$, and $|C_{h\gamma\gamma}|$ are centered around 0.93, 0.93, 0.95, 0.93, and 1.04, respectively, in interpreting the excesses at the 2σ level. They agree with the SM predictions within 10% uncertainties. $\mathrm{Br}(h \to b\bar{b})$ varies from 55.5% to 58.2%, coinciding with its SM prediction of $(57.7 \pm 1.8)\%$ [86]. In addition, although $\mathrm{Br}(h \to \gamma\gamma)$ changes from 3.07×10^{-3} to 3.16×10^{-3}, significantly larger than its SM prediction of $(2.28 \pm 0.11) \times 10^{-3}$ [86], the diphoton signal of h is comparable with its SM prediction.

We verified that the mass of the charged Higgs boson varied from 930 GeV to 3 TeV, where the lower bound came from the restrictions of the LHC searches for extra Higgs bosons and the upper bound relied on the explored parameter space.

2. Singlino-dominated DM case

We studied the $\tilde{S}$-dominated DM case similarly. We showed the distributions of various parameters in Figs. 6–8 and illustrated the Higgs properties in Figs. 9 and 10. We learned the following differences after comparing these figures with their corresponding ones for the $\tilde{B}$-dominated DM case:

(1) The $\tilde{S}$-dominated DM achieved the measured abundance mainly by coannihilating with higgsinolike (in most cases) or winolike electroweakinos. Since the cross sections for the scattering of the $\tilde{S}$-dominated DM with nucleons were different from those for the $\tilde{B}$-dominated DM, as indicated by Eq. (2.30) of Ref. [64], the LZ experiment allowed a moderately small $\mu_{\rm tot}$ even in the singlino-higgsino coannihilation case. Consequently, the posterior PDF preferred the spectrum pattern characterized by relatively small $|m_N|$ and $\mu_{\rm tot}$ together with larger $|M_1|$ and M_2, as shown in Fig. 7. It also preferred a larger λ than the prediction of the $\tilde{B}$-dominated DM case and subsequently a larger $V^{\rm NSM}_{h_s}$, as indicated in Eqs. (2.17) and (2.18). This feature was crucial for the case to

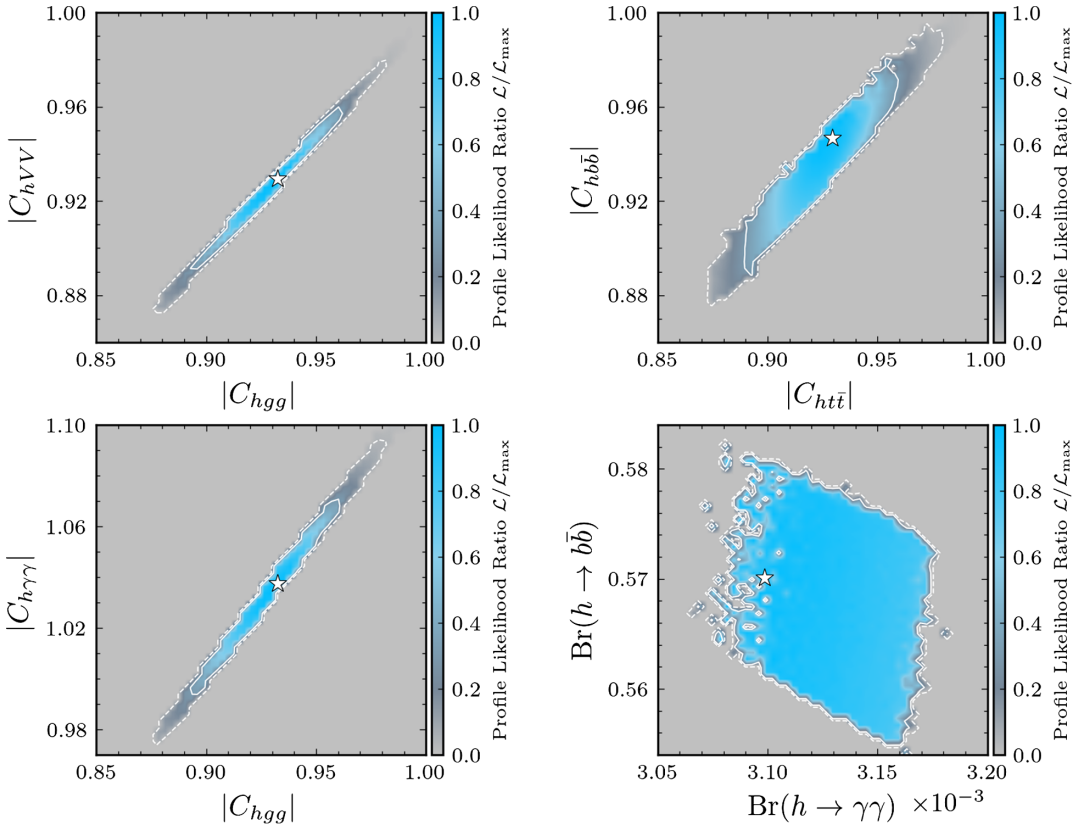

FIG. 5. Same as Fig. 4, but projected onto $|C_{hVV}| - |C_{hgg}|$, $|C_{hb\bar{b}}| - |C_{ht\bar{t}}|$, $|C_{h\gamma\gamma}| - |C_{hgg}|$, and $\mathrm{Br}(h \to b\bar{b}) - \mathrm{Br}(h \to \gamma\gamma)$ planes.

acquire the experimental values of $\mu_{\gamma\gamma}$ and $\mu_{b\bar{b}}$. In addition, given that the t-channel h_s-mediated contribution to the SI DM-nucleon scattering might be crucial with its amplitude proportional to $\kappa V_{h_s}^{\mathrm{SM}}$ in the leading-order approximation [64], the LZ results preferred a small κ. Figure 6 exhibits this feature.

Notably, the $\tilde{S}$-dominated DM can permanently annihilate into the $h_s h_s$ state. It may also annihilate into the $h_s A_s$ state if the kinematics is accessible. However, these annihilation channels are never dominant since κ is not significant [64]. Besides, the DM may achieve the measured density by the A_s-mediated resonant annihilation. This case contributes to the total Bayesian evidence by about 0.2%, very small because it needs the tuning of m_N and m_{A_s} to satisfy $m_N \simeq m_{A_s}/2$.

(2) Since the $\tilde{S}$-dominated DM had very weak couplings to the other sparticles, the heavy ones, except for the next-to-lightest sparticle (NLSP), were unlikely to directly decay into the DM. As a result, their decay chains were usually lengthened, which complicated the SUSY search. Concerning the coannihilation cases, however, one might simplify the situation. Specifically, the particle X in the decay $\mathrm{NLSP} \to \mathrm{DM} + \mathrm{X}$ was too soft to be detected by Strategy II, and thus, the NLSP behaves as the missing momentum at the LHC, the same as the DM signal. Consequently, the LHC search for SUSY had no exclusion capability on the samples after comparing the sparticle spectrum in Fig. 8 with the last two panels in Fig. 14 of Ref. [130], given that the DM and its coannihilation partners were massive, i.e., $m_{\tilde{\chi}^0_{1,2}}$, $m_{\tilde{\chi}^\pm_1} \gtrsim 300$ GeV with $m_{\tilde{\chi}^0_2} \simeq m_{\tilde{\chi}^\pm_1} \simeq m_{\tilde{\chi}^0_1}$ for the singlino-wino coannihilation case and $m_{\tilde{\chi}^0_{1,2,3}}$, $m_{\tilde{\chi}^\pm_1} \gtrsim 400$ GeV with $m_{\tilde{\chi}^0_2} \simeq m_{\tilde{\chi}^0_3} \simeq m_{\tilde{\chi}^\pm_1} \simeq m_{\tilde{\chi}^0_1}$ for the singlino-higgsino coannihilation case. We added that Strategy I also failed to exclude the compressed mass spectrum of the $\tilde{S}$-dominated DM case, again because the DM was massive. Furthermore, we studied some samples expected to leave remarkable signals at the LHC. Our simulation with the package CheckMATE-2.0.26 revealed that the R values were usually less than 0.5.

(3) Comparing Figs. 4 and 9 indicated that the 2σ confidence intervals for the $\tilde{S}$-dominated DM case were slightly larger than those for the $\tilde{B}$-dominated DM case, and the $\chi^2_{\gamma\gamma+b\bar{b}}$ for the best point of the former case was significantly smaller than that of the latter case. These observations revealed that the

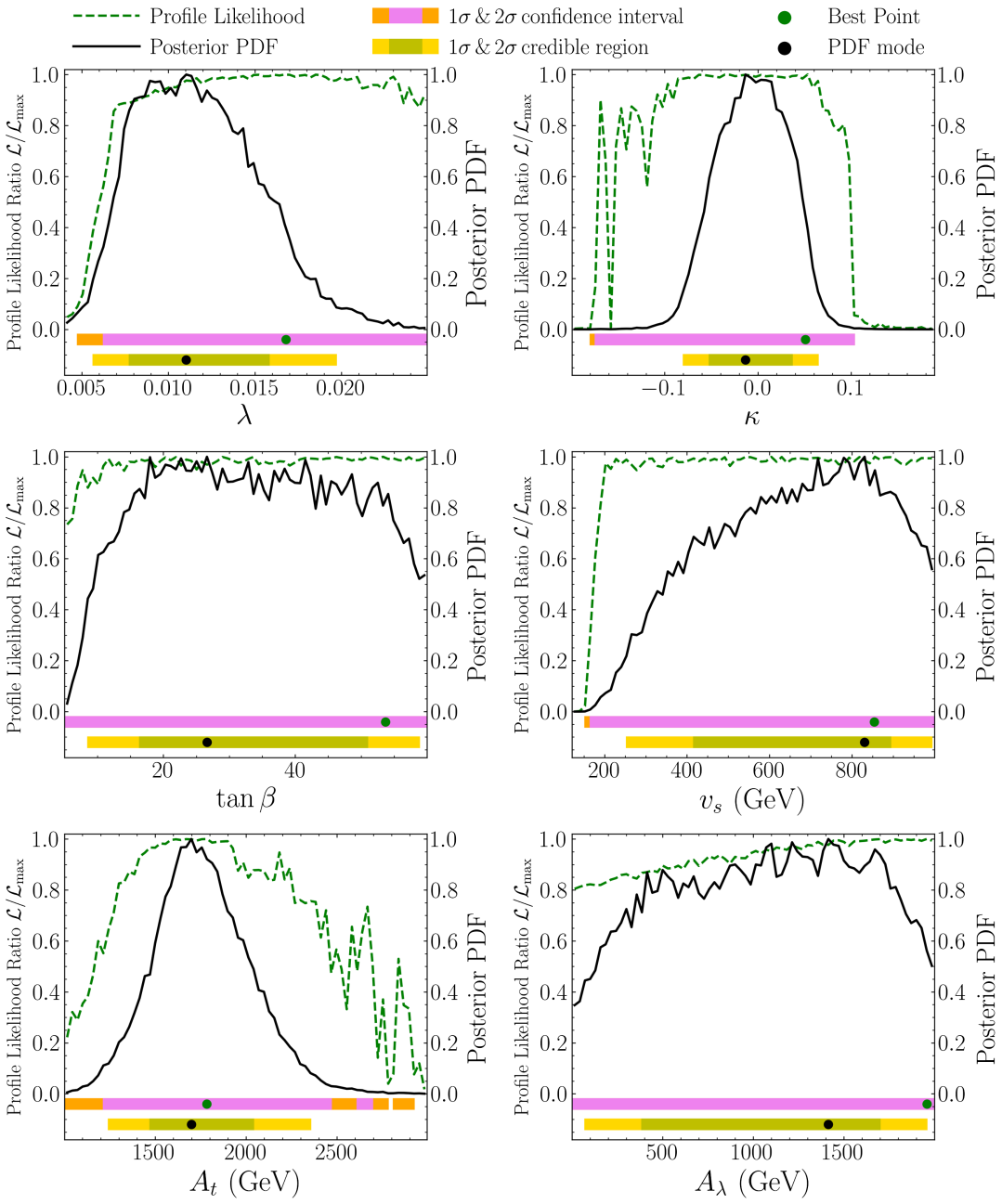

FIG. 6. Same as Fig. 1, but for the $\tilde{S}$-dominated DM case and $\chi^2_{\gamma\gamma+b\bar{b}} \simeq 0$ for the best point.

$\tilde{S}$-dominated DM case was more suited to explain the excesses. One primary reason was that the $\tilde{S}$-dominated DM case allowed a larger λ and a smaller $\mu_{\rm tot}$. It could predict a significant $V_{h_s}^{\rm NSM}$ and slightly enhance the supersymmetric contribution to $C_{h_s\gamma\gamma}$. Both could mitigate the substantial suppression of $C_{h_s b\bar{b}}$ and weaken the correlation between $\mu_{\gamma\gamma}$ and $\mu_{b\bar{b}}$. They make the case more accessible to explain the excess.

3. Status of the excesses

We summarize the status of the excesses in the GNMSSM. In Fig. 11, we projected all the samples obtained from the scan and adhered to experimental constraints onto the $\mu_{b\bar{b}} - \mu_{\gamma\gamma}$ planes. The left and right panels are for the $\tilde{B}$- and $\tilde{S}$-dominated DM cases, respectively, and the colors distinguish the dominant annihilation channels. This figure reveals that $\mu_{\gamma\gamma}$ and $\mu_{b\bar{b}}$ can reach 0.39 and 0.25, respectively, and their ratio, expressed as

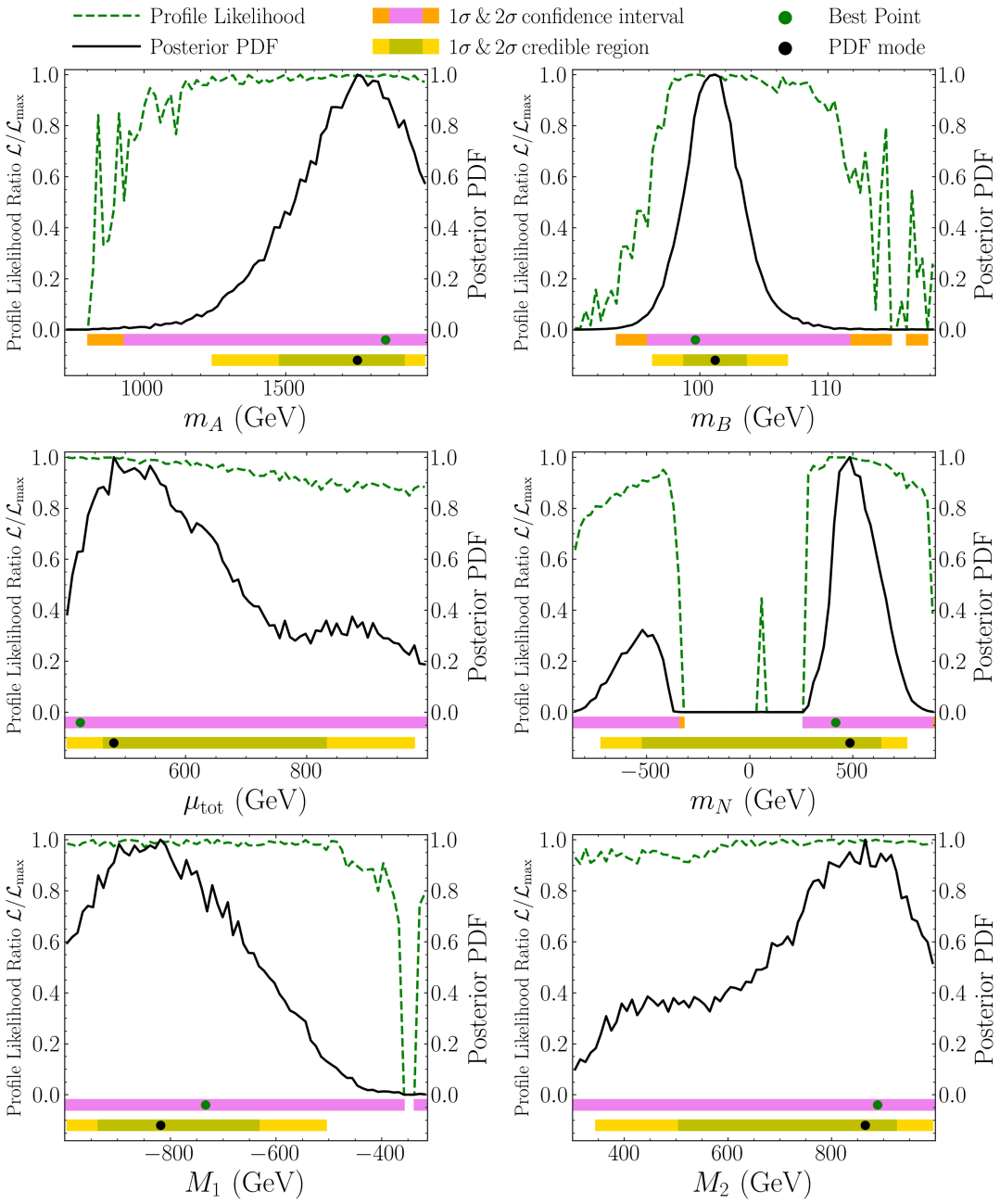

FIG. 7. Same as Fig. 2, but for the $\tilde{S}$-dominated DM case.

$$\frac{\mu_{\gamma\gamma}}{\mu_{b\bar{b}}} \equiv \frac{|C_{h_s gg}|^2}{|C_{h_s VV}|^2} \times \frac{|C_{h_s\gamma\gamma}|^2}{|C_{h_s b\bar{b}}|^2} \simeq \frac{|C_{h_s\gamma\gamma}|^2}{|C_{h_s b\bar{b}}|^2}, \tag{3.2}$$

varies from 1.2 to 1.7 for the $\tilde{B}$-dominated DM case and 1.2 to 2.5 for the $\tilde{S}$-dominated DM case. These conclusions indicate that the GNMSSM can easily explain the diphoton and $b\bar{b}$ excesses at the 1σ level. In particular, the $\tilde{S}$-dominated DM case can predict the central values of the signal strengths for the excesses. We verified that allowing A_λ to vary within a broader range than that in Table I could enhance the maximum reach of the ratio and improve the GNMSSM's capability to explain the excesses.

To further illuminate the physics underlying the excesses, we presented in Table II the details of two benchmark points, which corresponded to the best points of the two types of DM cases, respectively. Both explain the diphoton and $b\bar{b}$ excesses at the 1σ level and agree well with the other experimental restrictions. Particularly, their R values are not much below 1, implying that they will be explored at the LHC by the electroweakino productions in future.

IV. IMPLICATIONS OF THE EXCESSES

The GNMSSM interpretation of the excesses will be tested at future linear colliders, either by searching for h_s

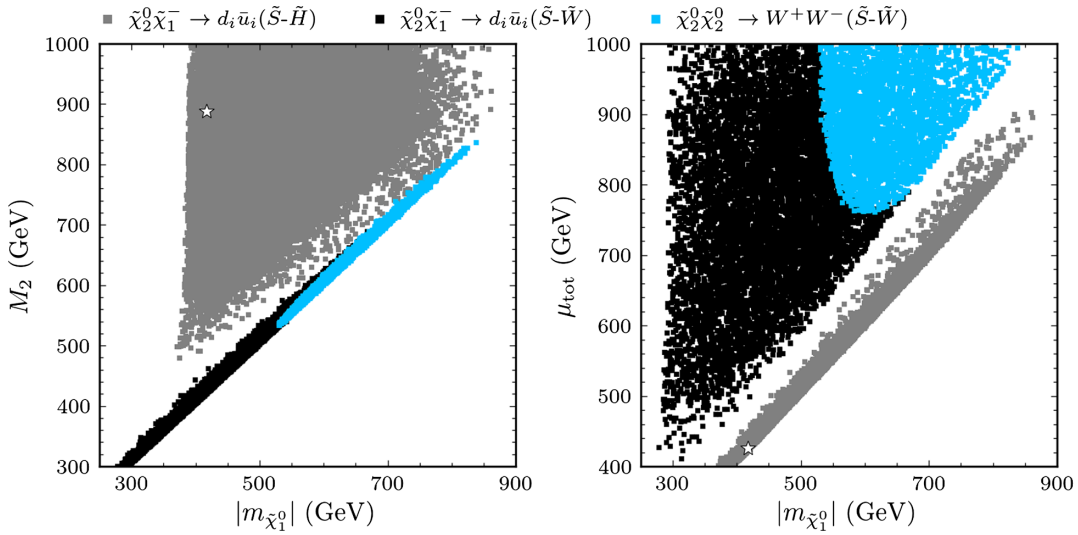

FIG. 8. Same as Fig. 3, but for the $\tilde{S}$-dominated DM case. It shows that the DM may be coannihilated with higgsinolike (in most cases) or winolike electroweakinos to acquire the measured density. The colors distinguish the dominant annihilation channels.

via the process $e^+e^- \to Zh_s$ and determining its properties or by precisely measuring the couplings of h [22]. It may also be explored by searching for the doublet-dominated Higgs bosons, H, A_H, and $H^\pm$, or the electroweakinos, assuming these particles are moderately light [24,33]. In this section, we briefly discuss the other signals of h_s at the LHC.

In Ref. [136], the CMS collaboration searched for the resonant production of a scalar X by the channel $pp \to X \to hY \to (\gamma\gamma)(b\bar{b})$ with an integrated luminosity of

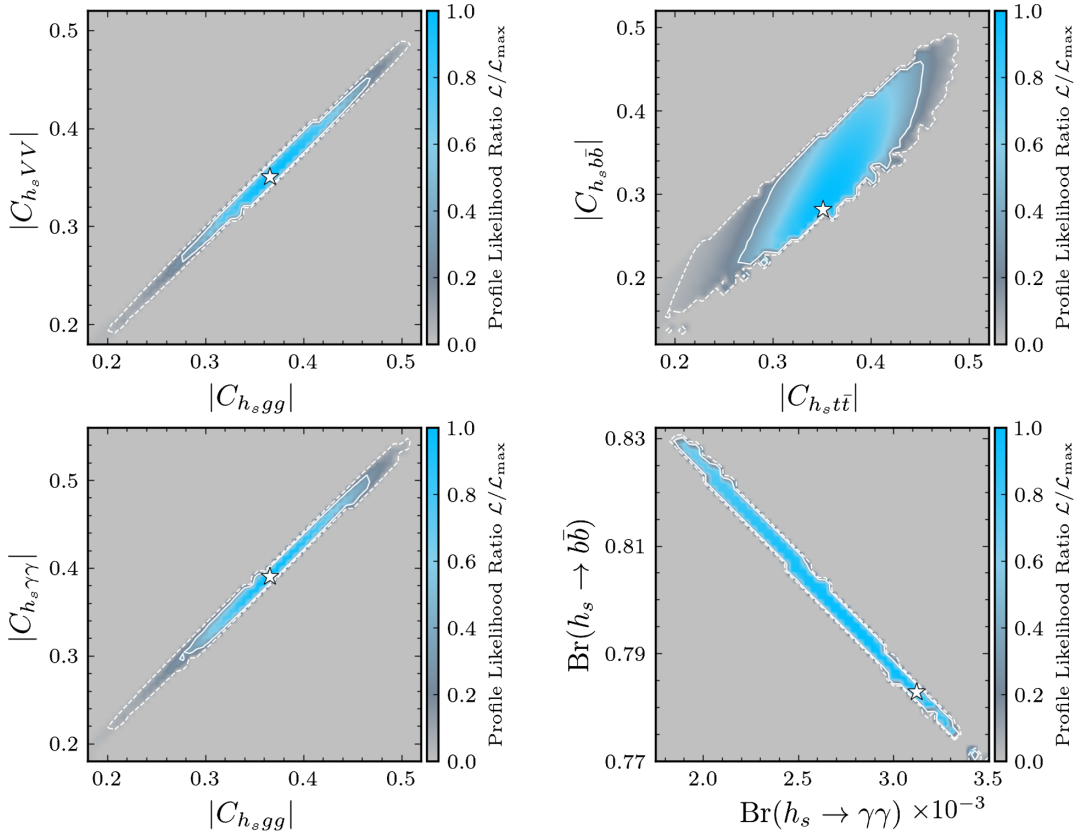

FIG. 9. Same as Fig. 4, but for the $\tilde{S}$-dominated DM case with $\chi^2_{\gamma\gamma+b\bar{b}} \simeq 0$ for the best point.

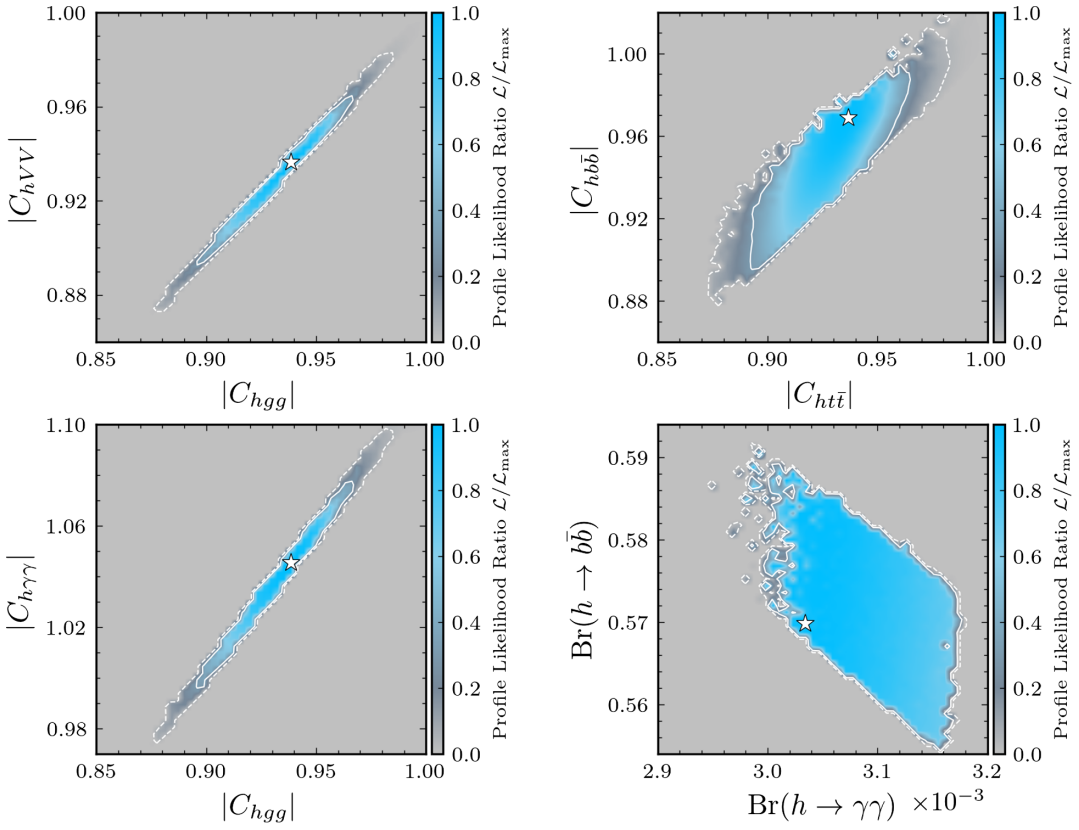

FIG. 10. Same as Fig. 5, but for the $\tilde{S}$-dominated DM case.

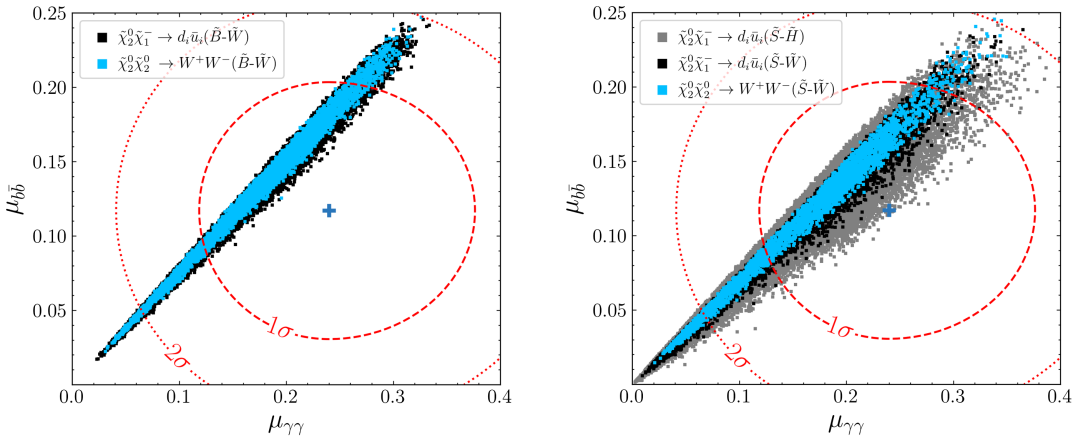

FIG. 11. Projection of the samples surviving the experimental restrictions onto the $\mu_{b\bar{b}} - \mu_{\gamma\gamma}$ planes. The left and right panels depict the pieces predicting $\tilde{B}$- and $\tilde{S}$-dominated DMs, respectively. The black and blue points represent the samples with $\tilde{\chi}_2^0\tilde{\chi}_1^- \to d_i\bar{u}_i$ ($i = 1, 2, 3$ denote the quark generations) and $\tilde{\chi}_2^0\tilde{\chi}_2^0 \to W^+W^-$ acting as the dominant annihilation channels in the bino-wino coannihilation case (left panel) and the singlino-wino coannihilation case (right panel), and the gray ones correspond to $\tilde{\chi}_2^0\tilde{\chi}_1^- \to d_i\bar{u}_i$ (i=1,2,3) as the dominant annihilation channel in the singlino-higgsino coannihilation case. Samples in the region enclosed by the red dashed and red dotted lines satisfy $\chi^2_{\gamma\gamma+b\bar{b}} \leq 2.30$ and $\chi^2_{\gamma\gamma+b\bar{b}} \leq 6.18$, respectively, indicating that they can explain the diphoton and $b\bar{b}$ excesses at the 1σ and 2σ levels.

TABLE II. Details of the best points for the $\tilde{B}$- and $\tilde{S}$-dominated DM cases, respectively. Both can explain the diphoton and $b\bar{b}$ excesses at the 1σ level and simultaneously be consistent with the other experimental restrictions. They achieved the measured abundance by coannihilating with the wino- and higgsino-dominated electroweakinos, respectively. d_i, u_i, and ℓ_i appear in the annihilation final state and denote the ith generation of down-type quarks, up-type quarks, and leptons, respectively.

Benchmark point P1				Benchmark point P2			
λ	0.012	m_{h_s}	96.0 GeV	λ	0.017	m_{h_s}	96.1 GeV
κ	0.133	m_h	125.1 GeV	κ	0.051	m_h	125.5 GeV
$\tan\beta$	56.41	m_H	2183 GeV	$\tan\beta$	53.71	m_H	2232 GeV
v_s	520.5 GeV	m_{A_s}	797.8 GeV	v_s	853.9 GeV	m_{A_s}	800.0 GeV
$\mu_{\rm tot}$	576.0 GeV	m_{A_H}	2183 GeV	$\mu_{\rm tot}$	425.7 GeV	m_{A_H}	2232 GeV
M_1	−294.0 GeV	$m_{H^\pm}$	2219 GeV	M_1	−733.0 GeV	$m_{H^\pm}$	2257 GeV
M_2	305.2 GeV	$m_{\tilde{\chi}_1^0}$	−293.9 GeV	M_2	888.3 GeV	$m_{\tilde{\chi}_1^0}$	417.2 GeV
A_t	1522 GeV	$m_{\tilde{\chi}_2^0}$	317.3 GeV	A_t	1784 GeV	$m_{\tilde{\chi}_2^0}$	432.6 GeV
A_λ	1589 GeV	$m_{\tilde{\chi}_3^0}$	−416.1 GeV	A_λ	1959 GeV	$m_{\tilde{\chi}_3^0}$	−436.8 GeV
m_A	1683 GeV	$m_{\tilde{\chi}_4^0}$	−595.3 GeV	m_A	1853 GeV	$m_{\tilde{\chi}_4^0}$	−741.3 GeV
m_B	105.82 GeV	$m_{\tilde{\chi}_5^0}$	601.9 GeV	m_B	99.65 GeV	$m_{\tilde{\chi}_5^0}$	930.7 GeV
m_N	−416.5 GeV	$m_{\tilde{\chi}_1^\pm}$	317.5 GeV	m_N	417.6 GeV	$m_{\tilde{\chi}_1^\pm}$	433.9 GeV
$\mu_{\gamma\gamma}$	0.206	$m_{\tilde{\chi}_2^\pm}$	604.4 GeV	$\mu_{\gamma\gamma}$	0.243	$m_{\tilde{\chi}_2^\pm}$	930.9 GeV
$\mu_{b\bar{b}}$	0.134	σ_p^{SI}	6.75×10^{-47}cm^2	$\mu_{b\bar{b}}$	0.116	σ_p^{SI}	1.07×10^{-46}cm^2
Ωh^2	0.113	σ_n^{SD}	1.55×10^{-42}cm^2	Ωh^2	0.131	σ_n^{SD}	5.60×10^{-45}cm^2
$V_{h_s}^S, V_{h_s}^{\rm SM}, V_{h_s}^{NSM}$		−0.929, 0.369, 4.5×10^{-4}		$V_{h_s}^S, V_{h_s}^{\rm SM}, V_{h_s}^{NSM}$		−0.936, 0.351, 1.3×10^{-3}	
$N_{11}, N_{12}, N_{13}, N_{14}, N_{15}$		0.994, 0.006, 0.097, 0.047, −0.002		$N_{11}, N_{12}, N_{13}, N_{14}, N_{15}$		0.004, 0.015, −0.092, 0.095, −0.991	
$N_{21}, N_{22}, N_{23}, N_{24}, N_{25}$		−0.007, −0.978, 0.184, −0.100, −0.001		$N_{21}, N_{22}, N_{23}, N_{24}, N_{25}$		−0.026, −0.113, 0.700, −0.691, −0.133	
$N_{31}, N_{32}, N_{33}, N_{34}, N_{35}$		−0.003, 0.001, 0.004, 0.007, −0.999		$N_{31}, N_{32}, N_{33}, N_{34}, N_{35}$		−0.101, −0.040, −0.704, −0.702, −0.002	
$N_{41}, N_{42}, N_{43}, N_{44}, N_{45}$		−0.102, 0.060, 0.698, 0.706, 0.008		$N_{41}, N_{42}, N_{43}, N_{44}, N_{45}$		0.995, −0.004, −0.052, −0.090, -0.000	
$N_{51}, N_{52}, N_{53}, N_{54}, N_{55}$		0.035, −0.201, −0.685, 0.699, 0.001		$N_{51}, N_{52}, N_{53}, N_{54}, N_{55}$		0.003, −0.993, −0.053, 0.109, 0.000	
$C_{h_sgg}, C_{h_sVV}, C_{h_s\gamma\gamma}, C_{h_st\bar{t}}, C_{h_sb\bar{b}}$		0.383, 0.369, 0.411, 0.369, 0.344		$C_{h_sgg}, C_{h_sVV}, C_{h_s\gamma\gamma}, C_{h_st\bar{t}}, C_{h_sb\bar{b}}$		0.366, 0.351, 0.391, 0.351, 0.281	
$C_{hgg}, C_{hVV}, C_{h\gamma\gamma}, C_{ht\bar{t}}, C_{hb\bar{b}}$		0.932, 0.929, 1.037, 0.929, 0.947		$C_{hgg}, C_{hVV}, C_{h\gamma\gamma}, C_{ht\bar{t}}, C_{hb\bar{b}}$		0.938, 0.936, 1.046, 0.936, 0.969	
Coannihilations		Fractions [%]		Coannihilations		Fractions [%]	
$\tilde{\chi}_2^0\tilde{\chi}_1^- \to d_i\bar{u}_i/ZW^-/\nu_{\ell_i}\bar{\ell}_i^-/A_sW^-$		29.3/6.5/10.2/1.7		$\tilde{\chi}_2^0\tilde{\chi}_1^- \to d_i\bar{u}_i/\nu_{\ell_i}\bar{\ell}_i^-/ZW^-/A_sW^-/hW^-$		21.8/8.0/1.3/1.3/1.1	
$\tilde{\chi}_2^0\tilde{\chi}_2^0 \to W^-W^+$		7.8		$\tilde{\chi}_3^0\tilde{\chi}_1^- \to d_i\bar{u}_i/\nu_{\ell_i}\bar{\ell}_i^-/ZW^-$		14.8/5.5/1.2	
Decays		Branching ratios [%]		Decays		Branching ratios [%]	
$\tilde{\chi}_2^0 \to \tilde{\chi}_1^0Z^*$		100		$\tilde{\chi}_2^0 \to \tilde{\chi}_1^0Z^*$		100	
$\tilde{\chi}_3^0 \to \tilde{\chi}_1^\pm W^\mp/\tilde{\chi}_1^0h_s$		86.8/10.2		$\tilde{\chi}_3^0 \to \tilde{\chi}_1^0Z^*$		98.1	
$\tilde{\chi}_4^0 \to \tilde{\chi}_1^\pm W^\mp/\tilde{\chi}_2^0Z/\tilde{\chi}_1^0h$		61.8/26.7/7.0		$\tilde{\chi}_4^0 \to \tilde{\chi}_1^\pm W^\mp/\tilde{\chi}_2^0Z/\tilde{\chi}_3^0h$		50.6/22.2/20.4	
$\tilde{\chi}_5^0 \to \tilde{\chi}_1^\pm W^\mp/\tilde{\chi}_2^0h/\tilde{\chi}_1^0Z$		63.1/21.1/8.3		$\tilde{\chi}_5^0 \to \tilde{\chi}_1^\pm W^\mp/\tilde{\chi}_3^0Z/\tilde{\chi}_2^0h$		51.4/21.9/18.3	
$\tilde{\chi}_1^+ \to \tilde{\chi}_1^0(W^+)^*$		100		$\tilde{\chi}_1^+ \to \tilde{\chi}_1^0(W^+)^*$		100	
$\tilde{\chi}_2^+ \to \tilde{\chi}_2^0W^+/\tilde{\chi}_1^+Z/\tilde{\chi}_1^+h/\tilde{\chi}_1^0W^+$		32.0/30.5/23.0/10.4		$\tilde{\chi}_2^+ \to \tilde{\chi}_3^0W^+/\tilde{\chi}_1^+Z/\tilde{\chi}_2^0W^+/\tilde{\chi}_1^+h$		25.4/25.1/25.0/21.2	
$h_s \to b\bar{b}/\tau^+\tau^-/gg/c\bar{c}/\gamma\gamma$		81.1/9.0/4.8/4.4/0.0024		$h_s \to b\bar{b}/\tau^+\tau^-/gg/c\bar{c}/\gamma\gamma$		78.3/8.7/6.3/5.8/0.0031	
$h \to b\bar{b}/WW^*/\tau^+\tau^-/gg/\gamma\gamma$		57.0/26.4/6.6/4.6/0.0031		$h \to b\bar{b}/WW^*/\tau^+\tau^-/gg/\gamma\gamma$		57.0/26.6/6.6/4.5/0.0030	
$H \to b\bar{b}/\tau^+\tau^-/\tilde{\chi}_1^+\tilde{\chi}_2^-/\tilde{\chi}_2^+\tilde{\chi}_1^-$		58.7/14.7/7.4/7.4		$H \to b\bar{b}/\tau^+\tau^-/\tilde{\chi}_1^+\tilde{\chi}_2^-/\tilde{\chi}_2^+\tilde{\chi}_1^-$		63.6/14.6/6.3/6.3	
$A_H \to b\bar{b}/\tau^+\tau^-$		80.2/12.2		$A_H \to b\bar{b}/\tau^+\tau^-$		86.6/13.2	
$H^+ \to t\bar{b}/\tau^+\nu_\tau/\tilde{\chi}_2^0\tilde{\chi}_2^+/\tilde{\chi}_5^0\tilde{\chi}_1^+/\tilde{\chi}_4^0\tilde{\chi}_1^+$		57.6/16.1/8.1/7.6/7.2		$H^+ \to t\bar{b}/\tau^+\nu_\tau/\tilde{\chi}_2^0\tilde{\chi}_2^+/\tilde{\chi}_5^0\tilde{\chi}_1^+/\tilde{\chi}_3^0\tilde{\chi}_2^+$		62.5/15.9/6.3/6.3/6.2	
R value: 0.17		Signal region: SR-WZoff-high-nja in Ref. [96]		R value: 0.35		Signal region: SR-4Q-VV in Ref. [130]	

138 fb^{-1} at $\sqrt{s} = 13$ TeV, where Y denoted another scalar satisfying $m_Y < m_X - m_h$. They acquired the 95% confidence level upper limits on the $\gamma\gamma b\bar{b}$ signal rate, ranging from 0.04 fb to 0.90 fb. Taking $X = H$ and $Y = h_s$ in the GNMSSM, the cross section of the $\gamma\gamma b\bar{b}$ signal is given by

$$\begin{aligned}\sigma_{\gamma\gamma b\bar{b}} &= (\sigma_{\rm SM}^{ggH}|C_{Hgg}|^2 + \sigma_{\rm SM}^{b\bar{b}H}|C_{Hb\bar{b}}|^2) \times {\rm Br}(H \to hh_s) \\ &\quad \times {\rm Br}(h \to \gamma\gamma) \times {\rm Br}(h_s \to b\bar{b}) \\ &\simeq (\sigma_{\rm SM}^{ggH} \times m_b^2/m_t^2 + \sigma_{\rm SM}^{b\bar{b}H}) \times \tan^2\beta \times {\rm Br}(H \to hh_s) \\ &\quad \times 0.228\% \times 76\%, \end{aligned} \tag{4.1}$$

in the large $\tan\beta$ case, where $\sigma_{\rm SM}^{ggH}$ and $\sigma_{\rm SM}^{b\bar{b}H}$ are the SM prediction of the H production rate via gluon-gluon and $b\bar{b}$ fusions, respectively, and ${\rm Br}(h_s \to b\bar{b}) \simeq 76\%$ as discussed in Sec. II B. If the decays of H into sparticles are kinematically forbidden, $H \to b\bar{b}$ will be the dominant decay channel, and thus ${\rm Br}(H \to hh_s) \simeq \Gamma(H \to hh_s)/\Gamma(H \to b\bar{b})$. Since $|V_H^{\rm NSM}| \simeq 1$, $|V_h^{\rm SM}| \simeq 1$, and $|V_{h_s}^{\rm S}| \simeq 1$, the Hhh_s coupling normalized by a factor of $-m_Z^2/v$ [90] can be acquired from Eq. (A.15) of Ref. [54]. It is $\lambda_{Hhh_s} \simeq \lambda(A_\lambda + m_N)v/m_Z^2 \simeq -m_A^2 V_{h_s}^{\rm NSM}/m_Z^2$, where we used the first approximation in Eq. (2.17) in the last step. Given $m_H \gg m_h$, we concluded that ${\rm Br}(H \to hh_s) \simeq m_H^2|V_{h_s}^{\rm NSM}|^2/(12m_b^2\tan^2\beta)$ by the width formulas in Ref. [90] and

$$\begin{aligned}\sigma_{\gamma\gamma b\bar{b}} &\simeq 7.1 \times 10^{-11} \times (5.8\sigma_{\rm SM}^{ggH} + 10^4\sigma_{\rm SM}^{b\bar{b}H}) \\ &\quad \times \left(\frac{m_H}{m_b\tan\beta}\right)^2 \times \left(\frac{V_{h_s}^{\rm NSM}\tan\beta}{0.07}\right)^2. \end{aligned} \tag{4.2}$$

These formulas indicate that on the premise of explaining the diphoton and $b\bar{b}$ excesses, $\sigma_{\gamma\gamma b\bar{b}} \simeq 0.026/\tan^2\beta$ fb for $m_H = 650$ GeV and $\sigma_{\gamma\gamma b\bar{b}} \simeq 0.014/\tan^2\beta$ fb for $m_H = 800$ GeV.[10] These cross sections are consistent with corresponding experimental bounds of 0.36 fb and 0.31 fb, respectively. Alternatively, the formulas imply that the GNMSSM fails to explain the diphoton and $b\bar{b}$ excesses and the 650 GeV excess reported in Ref. [136], which corresponds to $\sigma_{\gamma\gamma b\bar{b}} = 0.35^{+0.17}_{-0.13}$ fb [48], simultaneously.

In Ref. [10], the CMS Collaboration presented the search for a new boson ϕ in $\tau\bar{\tau}$ final states, using the data samples collected in the full Run 2 phase of the LHC. It acquired 95% confidence level bounds on the signal cross section, which was 12.2 pb for $m_\phi = 95$ GeV, corresponding to $\mu_{\tau\bar{\tau}}^{\rm exp} = 2.15$. As discussed in Sec. II B, the GNMSSM prediction of $\mu_{\tau\bar{\tau}}$ is around 0.11 if one intends to explain the diphoton and $b\bar{b}$ excesses. It is much smaller than the bound. It is also significantly lower than the signal rate needed to explain the $\tau\bar{\tau}$ excess observed in [10], which is $\mu_{\tau\bar{\tau}} = 1.38^{+0.69}_{-0.55}$ [48].

[10]In selecting these benchmark values of m_H, we do not consider the restrictions from the LHC searches for extra Higgs bosons by $\tau\bar{\tau}$ signal, which have set a bound of $m_H \gtrsim 930$ GeV in this study.

V. CONCLUSION

The CMS and ATLAS Collaborations recently published their results searching for light Higgs bosons, using the complete Run 2 data of the LHC. Both reported an excess in the diphoton invariant mass distribution at $m_{\gamma\gamma} \simeq 95.4$ GeV with compatible signal strengths. These observations confirmed the excess previously reported by CMS, which was based on the analyses of the Run 1 data of the LHC and the first year of the Run 2 data. The combined result increased the local significance to 3.1σ. Besides, the invariant mass of the diphoton signal coincided with that of the $b\bar{b}$ excess observed at the LEP. Although these excesses might originate from fluctuating much more extensive backgrounds, it is inspiring to speculate that they arise from a CP-even Higgs boson with its mass around 95.4 GeV. If this thought proves true, it will be the first sign of new physics in the Higgs sector.

Given the remarkable theoretical advantages of the GNMSSM, we explained the excesses by the resonant productions of the singlet-dominated scalar, h_s, predicted by the theory. We proposed a new set of input parameters to acquire simple approximations of the signal strengths in a large $\tan\beta$ limit. With the help of these formulas, we learned the dependence of the excesses on the model parameters such as λ, $\mu_{\rm tot}$, m_A, m_B, and A_λ. We also concluded that the central values of the signal strengths for the excesses corresponded to a moderately large SM Higgs field component in h_s and a suppressed $h_s b\bar{b}$ coupling compared with the $h_s t\bar{t}$ coupling, i.e., $V_{h_s}^{\rm SM} \simeq 0.36$, $C_{h_s t\bar{t}} \simeq 0.36$, and $C_{h_s b\bar{b}} \simeq 0.25$. In particular, we showed that the small deviations of $C_{h_s gg}$ and $C_{h_s\gamma\gamma}$ from $C_{h_s t\bar{t}}$ could alleviate the suppression of the $h_s b\bar{b}$ couplings by significantly reducing the $H_{\rm NSM}$ component in h_s and thus make the theory more accessible to explain the excesses. These observations guided us to find the parameter space responsible for the excesses.

We performed a sophisticated scan over the broad parameter space of the GNMSSM to investigate the impacts of various experimental restrictions, including those from the 125 GeV Higgs data, the DM relic abundance and direct detection experiments, and the collider searches for SUSY and extra Higgs bosons, on the explanations. After analyzing the distributions of different parameters, we had the following conclusions:

(1) Present 125 GeV Higgs data, and the collider searches for extra Higgs bosons were compatible with the existence of the light singlet-dominated Higgs boson responsible for the excesses. They

influenced the Higgs physics only by setting lower bounds on the mass of charged Higgs bosons.

(2) The DM physics could affect the explanations by determining the PLs and posterior PDFs of some parameters crucial for the excesses, such as λ and $\mu_{\rm tot}$. Specifically, the DM candidate might be $\tilde{B}$ or $\tilde{S}$ dominated $\tilde{\chi}_1^0$. The $\tilde{B}$-dominated DM achieved the measured relic abundance mainly by coannihilating with the winolike electroweakinos. A small λ and a sufficiently large $\mu_{\rm tot}$ characterized this case in accounting for the excesses and simultaneously satisfying the restrictions from the DM direct detection experiments. Consequently, $V_{h_s}^{\rm NSM}$ was minor, and the chargino's contribution to $C_{h_s\gamma\gamma}$ was never significant. By contrast, the $\tilde{S}$-dominated DM could obtain the correct abundance by coannihilating with the higgsinolike or winolike electroweakinos. This case allowed a larger λ and a smaller $\mu_{\rm tot}$ to provide a significant $V_{h_s}^{\rm NSM}$ and also enhance the supersymmetric contributions to $C_{h_s\gamma\gamma}$. As a result, the $\tilde{S}$-dominated DM case is slightly more suited to explain the excesses.

(3) The GNMSSM primarily relied on the Higgs mixings instead of significant supersymmetric contributions to C_{h_sgg} and $C_{h_s\gamma\gamma}$ to explain the excesses. Given that this mechanism could be realized even for massive sparticles, the explanation possessed broad parameter space consistent with the LHC searches for SUSY by either Strategy I or II. We verified this point by simulating some samples expected to have distinguished signals at the LHC.

(4) Given the parameter space of the GNMSSM in Table I, the signal strengths $\mu_{\gamma\gamma}$ and $\mu_{b\bar{b}}$ could reach 0.36 and 0.25 without conflicting the experimental restrictions. Their ratio varied from 1.2 to 1.7 for the $\tilde{B}$-dominated DM case and 1.2 to 2.5 for the $\tilde{S}$-dominated DM case. Consequently, the GNMSSM could simultaneously explain the diphoton and $b\bar{b}$ excesses at the 1σ level. In particular, the $\tilde{S}$-dominated DM case could predict the central values of the signal strengths for the excesses.

We add that our explanation predicts the cross sections of the $\gamma\gamma b\bar{b}$ signal from process $pp \to H \to h_s h$ at the LHC and the $\tau\bar{\tau}$ signal from the production $pp \to h_s \to \tau\bar{\tau}$ in simple forms that are consistent with corresponding experimental bounds. We look forward to seeing that the run 3 results from ATLAS and CMS and future runs of the high luminosity LHC could illuminate whether the excesses persist and arise from a BSM particle. We expect that future linear colliders could provide definite conclusions on these excesses.

ACKNOWLEDGMENTS

We thank Dr. Junquan Tao for helpful discussions about the details of the diphoton excess observed by the CMS Collaboration. This work is supported by the National Natural Science Foundation of China (NNSFC) under Grant No. 12075076.

[1] CMS Collaboration, Search for new resonances in the diphoton final state in the mass range between 80 and 115 GeV in pp collisions at $\sqrt{s} = 8$ TeV, Report No. CMS-PAS-HIG-14-037, 2015.

[2] A. M. Sirunyan *et al.* (CMS Collaboration), Search for a standard model-like Higgs boson in the mass range between 70 and 110 GeV in the diphoton final state in proton-proton collisions at $\sqrt{s} = 8$ and 13 TeV, Phys. Lett. B **793**, 320 (2019).

[3] CMS Collaboration, Search for a standard model-like Higgs boson in the mass range between 70 and 110 GeV in the diphoton final state in proton-proton collisions at $\sqrt{s} = 13$ TeV, Report No. CMS-PAS-HIG-20-002, 2023.

[4] ATLAS Collaboration, Search for resonances in the 65 to 110 GeV diphoton invariant mass range using 80 fb^{-1} of pp collisions collected at $\sqrt{s} = 13$ TeV with the ATLAS detector, Report No. ATLAS-CONF-2018-025, 7, 2018.

[5] C. Arcangeletti (on behalf of ATLAS Collaboration), LHC Seminar (2023), https://indico.cern.ch/event/1281604/attachments/2660420/4608571/LHCSeminarArcangeletti-final.pdf.

[6] T. Biekötter, S. Heinemeyer, and G. Weiglein, The 95.4 GeV di-photon excess at ATLAS and CMS, Phys. Rev. D **109**, 035005 (2024).

[7] R. Barate *et al.* (LEP Working Group for Higgs boson searches, ALEPH, DELPHI, L3, OPAL Collaborations), Search for the standard model Higgs boson at LEP, Phys. Lett. B **565**, 61 (2003).

[8] A. Azatov, R. Contino, and J. Galloway, Model-independent bounds on a light Higgs, J. High Energy Phys. 04 (2012) 127.

[9] J. Cao, X. Guo, Y. He, P. Wu, and Y. Zhang, Diphoton signal of the light Higgs boson in natural NMSSM, Phys. Rev. D **95**, 116001 (2017).

[10] A. Tumasyan *et al.* (CMS Collaboration), Searches for additional Higgs bosons and for vector leptoquarks in $\tau\tau$

final states in proton-proton collisions at $\sqrt{s} = 13$ TeV, J. High Energy Phys. 07 (2023) 073.
[11] G. Coloretti, A. Crivellin, S. Bhattacharya, and B. Mellado, Searching for low-mass resonances decaying into W bosons, Phys. Rev. D **108**, 035026 (2023).
[12] S. Heinemeyer and T. Stefaniak, A Higgs boson at 96 GeV?!, Proc. Sci. CHARGED2018 (**2019**) 016.
[13] S. Ashanujjaman, S. Banik, G. Coloretti, A. Crivellin, B. Mellado, and A.-T. Mulaudzi, $SU(2)_L$ triplet scalar as the origin of the 95 GeV excess?, Phys. Rev. D **108**, L091704 (2023).
[14] J. A. Aguilar-Saavedra and F. R. Joaquim, Multiphoton signals of a (96 GeV?) stealth boson, Eur. Phys. J. C **80**, 403 (2020).
[15] A. Kundu, S. Maharana, and P. Mondal, A 96 GeV scalar tagged to dark matter models, Nucl. Phys. **B955**, 115057 (2020).
[16] P. J. Fox and N. Weiner, Light signals from a lighter Higgs, J. High Energy Phys. 08 (2018) 025.
[17] A. Belyaev, R. Benbrik, M. Boukidi, M. Chakraborti, S. Moretti, and S. Semlali, Explanation of the hints for a 95 GeV Higgs boson within a 2-Higgs doublet model, arXiv:2306.09029.
[18] D. Azevedo, T. Biekötter, and P. M. Ferreira, 2HDM interpretations of the CMS diphoton excess at 95 GeV, J. High Energy Phys. 11 (2023) 017.
[19] R. Benbrik, M. Boukidi, and B. Manaut, W-mass and 96 GeV excess in type-III 2HDM, arXiv:2204.11755.
[20] R. Benbrik, M. Boukidi, S. Moretti, and S. Semlali, Explaining the 96 GeV Di-photon anomaly in a generic 2HDM Type-III, Phys. Lett. B **832**, 137245 (2022).
[21] U. Haisch and A. Malinauskas, Let there be light from a second light Higgs doublet, J. High Energy Phys. 03 (2018) 135.
[22] T. Biekötter, M. Chakraborti, and S. Heinemeyer, An N2HDM solution for the possible 96 GeV excess, Proc. Sci. CORFU2018 (**2019**) 015.
[23] T. Biekötter, M. Chakraborti, and S. Heinemeyer, A 96 GeV Higgs boson in the N2HDM, Eur. Phys. J. C **80**, 2 (2020).
[24] T. Biekötter, M. Chakraborti, and S. Heinemeyer, The 96 GeV excess at the LHC, Int. J. Mod. Phys. A **36**, 2142018 (2021).
[25] T. Biekötter, A. Grohsjean, S. Heinemeyer, C. Schwanenberger, and G. Weiglein, Possible indications for new Higgs bosons in the reach of the LHC: N2HDM and NMSSM interpretations, Eur. Phys. J. C **82**, 178 (2022).
[26] T. Biekötter and M. O. Olea-Romacho, Reconciling Higgs physics and pseudo-Nambu-Goldstone dark matter in the S2HDM using a genetic algorithm, J. High Energy Phys. 10 (2021) 215.
[27] S. Heinemeyer, C. Li, F. Lika, G. Moortgat-Pick, and S. Paasch, Phenomenology of a 96 GeV Higgs boson in the 2HDM with an additional singlet, Phys. Rev. D **106**, 075003 (2022).
[28] T. Biekötter, S. Heinemeyer, and G. Weiglein, Mounting evidence for a 95 GeV Higgs boson, J. High Energy Phys. 08 (2022) 201.
[29] C. Li, Phenomenology of extended Two-Higgs-Doublets models, Ph.D. thesis, Hamburg U., 2023.
[30] T. Biekötter, S. Heinemeyer, and G. Weiglein, The CMS di-photon excess at 95 GeV in view of the LHC Run 2 results, Phys. Lett. B **846**, 138217 (2023).
[31] J. A. Aguilar-Saavedra, H. B. Câmara, F. R. Joaquim, and J. F. Seabra, Confronting the 95 GeV excesses within the UN2HDM, Phys. Rev. D **108**, 075020 (2023).
[32] S. Banik, A. Crivellin, S. Iguro, and T. Kitahara, Asymmetric Di-Higgs signals of the N2HDM-$U(1)$, Phys. Rev. D **108**, 075011 (2023).
[33] J. Dutta, J. Lahiri, C. Li, G. Moortgat-Pick, S. F. Tabira, and J. A. Ziegler, Dark matter phenomenology in 2HDMS in light of the 95 GeV excess, arXiv:2308.05653.
[34] D. Sachdeva and S. Sadhukhan, Discussing 125 GeV and 95 GeV excess in light radion model, Phys. Rev. D **101**, 055045 (2020).
[35] R. Vega, R. Vega-Morales, and K. Xie, Light (and darkness) from a light hidden Higgs, J. High Energy Phys. 06 (2018) 137.
[36] J.-W. Fan, J.-Q. Tao, Y.-Q. Shen, G.-M. Chen, H.-S. Chen, S. Gascon-Shotkin, M. Lethuillier, L. Sgandurra, and P. Soulet, Study of diphoton decays of the lightest scalar Higgs boson in the next-to-minimal supersymmetric standard model, Chin. Phys. C **38**, 073101 (2014).
[37] S. Heinemeyer, A Higgs boson below 125 GeV?!, Int. J. Mod. Phys. A **33**, 1844006 (2018).
[38] C. Beskidt, W. de Boer, and D. I. Kazakov, Can we discover a light singlet-like NMSSM Higgs boson at the LHC?, Phys. Lett. B **782**, 69 (2018).
[39] A. A. Abdelalim, B. Das, S. Khalil, and S. Moretti, Diphoton decay of a light Higgs state in the BLSSM, Nucl. Phys. **B985**, 116013 (2022).
[40] W. G. Hollik, C. Li, G. Moortgat-Pick, and S. Paasch, Phenomenology of a supersymmetric model inspired by inflation, Eur. Phys. J. C **81**, 141 (2021).
[41] J. Cao, X. Jia, Y. Yue, H. Zhou, and P. Zhu, 96 GeV diphoton excess in seesaw extensions of the natural NMSSM, Phys. Rev. D **101**, 055008 (2020).
[42] T. Biekötter, S. Heinemeyer, and C. Muñoz, Precise prediction for the Higgs-boson masses in the $\mu\nu$ SSM with three right-handed neutrino superfields, Eur. Phys. J. C **79**, 667 (2019).
[43] T. Biekötter, S. Heinemeyer, and C. Muñoz, Precise prediction for the Higgs-boson masses in the $\mu\nu$ SSM, Eur. Phys. J. C **78**, 504 (2018).
[44] K. Choi, S. H. Im, K. S. Jeong, and C. B. Park, Light Higgs bosons in the general NMSSM, Eur. Phys. J. C **79**, 956 (2019).
[45] K. Wang, F. Wang, J. Zhu, and Q. Jie, The semi-constrained NMSSM in light of muon g-2, LHC, and dark matter constraints, Chin. Phys. C **42**, 103109 (2018).
[46] F. Domingo, S. Heinemeyer, S. Paßehr, and G. Weiglein, Decays of the neutral Higgs bosons into SM fermions and gauge bosons in the $\mathcal{CP}$-violating NMSSM, Eur. Phys. J. C **78**, 942 (2018).
[47] W. Li, J. Zhu, K. Wang, S. Ma, P. Tian, and H. Qiao, A light Higgs boson in the NMSSM confronted with the CMS di-photon and di-tau excesses, Chin. Phys. C **47**, 123102 (2023).

[48] U. Ellwanger and C. Hugonie, Additional Higgs Bosons near 95 and 650 GeV in the NMSSM, Eur. Phys. J. C **83**, 1138 (2023).
[49] F. Richard, Search for a light radion at HL-LHC and ILC250, arXiv:1712.06410.
[50] D. Liu, J. Liu, C. E. M. Wagner, and X.-P. Wang, A light Higgs at the LHC and the B-anomalies, J. High Energy Phys. 06 (2018) 150.
[51] J. M. Cline and T. Toma, Pseudo-Goldstone dark matter confronts cosmic ray and collider anomalies, Phys. Rev. D **100**, 035023 (2019).
[52] P. Escribano, V. M. Lozano, and A. Vicente, A scotogenic explanation for the 95 GeV excesses, Phys. Rev. D **108**, 115001 (2023).
[53] D. Borah, S. Mahapatra, P. K. Paul, and N. Sahu, Scotogenic $U(1)_{L_\mu - L_\tau}$ origin of $(g-2)_\mu$, W-mass anomaly and 95 GeV excess, arXiv:2310.11953.
[54] U. Ellwanger, C. Hugonie, and A. M. Teixeira, The next-to-minimal supersymmetric standard model, Phys. Rep. **496**, 1 (2010).
[55] J. Aalbers *et al.* (LUX-ZEPLIN Collaboration), First dark matter search results from the LUX-ZEPLIN (LZ) experiment, Phys. Rev. Lett. **131**, 041002 (2023).
[56] Y. He, X. Jia, L. Meng, Y. Yue, and D. Zhang, Impact of recent measurement of $(g-2)_\mu$, LHC search for supersymmetry, and LZ experiment on minimal supersymmetric standard model, Phys. Rev. D **108**, 115010 (2023).
[57] G. F. Giudice and A. Masiero, A natural solution to the mu problem in supergravity theories, Phys. Lett. B **206**, 480 (1988).
[58] A. Arvanitaki, M. Baryakhtar, X. Huang, K. van Tilburg, and G. Villadoro, The last vestiges of naturalness, J. High Energy Phys. 03 (2014) 022.
[59] J. A. Evans, Y. Kats, D. Shih, and M. J. Strassler, Toward full LHC coverage of natural supersymmetry, J. High Energy Phys. 07 (2014) 101.
[60] H. Baer, V. Barger, D. Mickelson, and M. Padeffke-Kirkland, SUSY models under siege: LHC constraints and electroweak fine-tuning, Phys. Rev. D **89**, 115019 (2014).
[61] P. Fayet, Supergauge invariant extension of the Higgs mechanism and a model for the electron and its neutrino, Nucl. Phys. **B90**, 104 (1975).
[62] P. Fayet and S. Ferrara, Supersymmetry, Phys. Rep. **32**, 249 (1977).
[63] U. Ellwanger and A. M. Teixeira, NMSSM with a singlino LSP: Possible challenges for searches for supersymmetry at the LHC, J. High Energy Phys. 10 (2014) 113.
[64] J. Cao, D. Li, J. Lian, Y. Yue, and H. Zhou, Singlino-dominated dark matter in general NMSSM, J. High Energy Phys. 06 (2021) 176.
[65] J. Cao, L. Meng, Y. Yue, H. Zhou, and P. Zhu, Suppressing the scattering of WIMP dark matter and nucleons in supersymmetric theories, Phys. Rev. D **101**, 075003 (2020).
[66] J. Cao, F. Ding, C. Han, J. M. Yang, and J. Zhu, A light Higgs scalar in the NMSSM confronted with the latest LHC Higgs data, J. High Energy Phys. 11 (2013) 018.
[67] S. Baum, M. Carena, N. R. Shah, and C. E. M. Wagner, Higgs portals for thermal dark matter. EFT perspectives and the NMSSM, J. High Energy Phys. 04 (2018) 069.
[68] U. Ellwanger and C. Hugonie, The higgsino–singlino sector of the NMSSM: Combined constraints from dark matter and the LHC, Eur. Phys. J. C **78**, 735 (2018).
[69] J. Cao, J. Lian, Y. Pan, D. Zhang, and P. Zhu, Improved $(g-2)_\mu$ measurement and singlino dark matter in μ-term extended Z_3-NMSSM, J. High Energy Phys. 09 (2021) 175.
[70] J. Cao, X. Jia, L. Meng, Y. Yue, and D. Zhang, Status of the singlino-dominated dark matter in general next-to-minimal supersymmetric standard model, J. High Energy Phys. 03 (2023) 198.
[71] U. Ellwanger, A Higgs boson near 125 GeV with enhanced di-photon signal in the NMSSM, J. High Energy Phys. 03 (2012) 044.
[72] M. Badziak, M. Olechowski, and S. Pokorski, New regions in the NMSSM with a 125 GeV Higgs, J. High Energy Phys. 06 (2013) 043.
[73] J.-J. Cao, Z.-X. Heng, J. M. Yang, Y.-M. Zhang, and J.-Y. Zhu, A SM-like Higgs near 125 GeV in low energy SUSY: A comparative study for MSSM and NMSSM, J. High Energy Phys. 03 (2012) 086.
[74] U. Ellwanger, Nonrenoralizable interaction from supergravity, quatum corrections and effective low-energy theories, Phys. Lett. **133B**, 187 (1983).
[75] S. A. Abel, Destabilizing divergences in the NMSSM, Nucl. Phys. **B480**, 55 (1996).
[76] C. F. Kolda, S. Pokorski, and N. Polonsky, Stabilized singlets in supergravity as a source of the mu—parameter, Phys. Rev. Lett. **80**, 5263 (1998).
[77] C. Panagiotakopoulos and K. Tamvakis, Stabilized NMSSM without domain walls, Phys. Lett. B **446**, 224 (1999).
[78] G. G. Ross and K. Schmidt-Hoberg, The fine-tuning of the generalised NMSSM, Nucl. Phys. **B862**, 710 (2012).
[79] H. M. Lee, S. Raby, M. Ratz, G. G. Ross, R. Schieren, K. Schmidt-Hoberg, and P. K. S. Vaudrevange, A unique $\mathbb{Z}_4^R$ symmetry for the MSSM, Phys. Lett. B **694**, 491 (2011).
[80] H. M. Lee, S. Raby, M. Ratz, G. G. Ross, R. Schieren, K. Schmidt-Hoberg *et al.*, Discrete R symmetries for the MSSM and its singlet extensions, Nucl. Phys. **B850**, 1 (2011).
[81] G. G. Ross, K. Schmidt-Hoberg, and F. Staub, The generalised NMSSM at one loop: Fine tuning and phenomenology, J. High Energy Phys. 08 (2012) 074.
[82] D. J. Miller, R. Nevzorov, and P. M. Zerwas, The Higgs sector of the next-to-minimal supersymmetric standard model, Nucl. Phys. **B681**, 3 (2004).
[83] ATLAS Collaboration, A detailed map of Higgs boson interactions by the ATLAS experiment ten years after the discovery, Nature (London) **607**, 52 (2022).
[84] A. Tumasyan *et al.* (CMS Collaboration), A portrait of the Higgs boson by the CMS experiment ten years after the discovery, Nature (London) **607**, 60 (2022).
[85] G. Aad *et al.* (ATLAS Collaboration), Search for heavy Higgs bosons decaying into two tau leptons with the

ATLAS detector using pp collisions at $\sqrt{s} = 13$ TeV, Phys. Rev. Lett. **125**, 051801 (2020).
[86] J. R. Andersen *et al.* (LHC Higgs Cross Section Working Group Collaboration), Handbook of LHC Higgs cross sections: 3. Higgs properties, arXiv:1307.1347.
[87] S. F. King, M. Mühlleitner, R. Nevzorov, and K. Walz, Natural NMSSM Higgs bosons, Nucl. Phys. **B870**, 323 (2013).
[88] W. Porod, SPheno, a program for calculating supersymmetric spectra, SUSY particle decays and SUSY particle production at $e+$ $e-$ colliders, Comput. Phys. Commun. **153**, 275 (2003).
[89] W. Porod and F. Staub, SPheno 3.1: Extensions including flavour, CP-phases and models beyond the MSSM, Comput. Phys. Commun. **183**, 2458 (2012).
[90] A. Djouadi, The anatomy of electro-weak symmetry breaking. II. The Higgs bosons in the minimal supersymmetric model, Phys. Rep. **459**, 1 (2008).
[91] A. Djouadi, The anatomy of electro-weak symmetry breaking. I: The Higgs boson in the standard model, Phys. Rep. **457**, 1 (2008).
[92] M. Spira, A. Djouadi, D. Graudenz, and P. M. Zerwas, Higgs boson production at the LHC, Nucl. Phys. **B453**, 17 (1995).
[93] F. Staub *et al.*, Precision tools and models to narrow in on the 750 GeV diphoton resonance, Eur. Phys. J. C **76**, 516 (2016).
[94] K. Choi, S. H. Im, K. S. Jeong, and M. Yamaguchi, Higgs mixing and diphoton rate enhancement in NMSSM models, J. High Energy Phys. 02 (2013) 090.
[95] M. Carena, D. Garcia, U. Nierste, and C. E. M. Wagner, Effective Lagrangian for the $\bar{t}bH^+$ interaction in the MSSM and charged Higgs phenomenology, Nucl. Phys. **B577**, 88 (2000).
[96] G. Aad *et al.* (ATLAS Collaboration), Search for chargino–neutralino pair production in final states with three leptons and missing transverse momentum in $\sqrt{s} = 13$ TeV pp collisions with the ATLAS detector, Eur. Phys. J. C **81**, 1118 (2021).
[97] F. Staub, SARAH, arXiv:0806.0538.
[98] F. Staub, SARAH 3.2: Dirac Gauginos, UFO output, and more, Comput. Phys. Commun. **184**, 1792 (2013).
[99] F. Staub, SARAH 4: A tool for (not only SUSY) model builders, Comput. Phys. Commun. **185**, 1773 (2014).
[100] F. Staub, Exploring new models in all detail with SARAH, Adv. High Energy Phys. **2015**, 840780 (2015).
[101] W. Porod, F. Staub, and A. Vicente, A flavor kit for BSM models, Eur. Phys. J. C **74**, 2992 (2014).
[102] G. Belanger, F. Boudjema, A. Pukhov, and A. Semenov, MicrOMEGAs: A Program for calculating the relic density in the MSSM, Comput. Phys. Commun. **149**, 103 (2002).
[103] G. Bélanger, F. Boudjema, A. Pukhov, and A. Semenov, MicrOMEGAs: Version 1.3, Comput. Phys. Commun. **174**, 577 (2006).
[104] G. Bélanger, F. Boudjema, C. Hugonie, A. Pukhov, and A. Semenov, Relic density of dark matter in the NMSSM, J. Cosmol. Astropart. Phys. 09 (2005) 001.
[105] G. Bélanger, F. Boudjema, A. Pukhov, and A. Semenov, MicrOMEGAs 2.0: A Program to calculate the relic density of dark matter in a generic model, Comput. Phys. Commun. **176**, 367 (2007).
[106] G. Bélanger, F. Boudjema, S. Kraml, A. Pukhov, and A. Semenov, Relic density of neutralino dark matter in the MSSM with CP violation, Phys. Rev. D **73**, 115007 (2006).
[107] G. Bélanger, F. Boudjema, A. Pukhov, and A. Semenov, Dark matter direct detection rate in a generic model with MicrOMEGAs 2.2, Comput. Phys. Commun. **180**, 747 (2009).
[108] G. Belanger, F. Boudjema, A. Pukhov, and A. Semenov, MicrOMEGAs: A tool for dark matter studies, Nuovo Cimento C **033N2**, 111 (2010).
[109] G. Bélanger, F. Boudjema, A. Pukhov, and A. Semenov, MicrOMEGAs_3: A program for calculating dark matter observables, Comput. Phys. Commun. **185**, 960 (2014).
[110] D. Barducci, G. Belanger, J. Bernon, F. Boudjema, J. Da Silva, S. Kraml *et al.*, Collider limits on new physics within MicrOMEGAs_4.3, Comput. Phys. Commun. **222**, 327 (2018).
[111] G. Bélanger, F. Boudjema, A. Goudelis, A. Pukhov, and B. Zaldivar, MicrOMEGAs5.0: Freezein, Comput. Phys. Commun. **231**, 173 (2018).
[112] A. Fowlie and M. H. Bardsley, Superplot: A graphical interface for plotting and analysing MultiNest output, Eur. Phys. J. Plus **131**, 391 (2016).
[113] F. Feroz, M. P. Hobson, and M. Bridges, MultiNest: An efficient and robust Bayesian inference tool for cosmology and particle physics, Mon. Not. R. Astron. Soc. **398**, 1601 (2009).
[114] F. Feroz, M. P. Hobson, E. Cameron, and A. N. Pettitt, Importance nested sampling and the MultiNest algorithm, Open J. Astrophys. **2**, 10 (2019).
[115] P. Athron *et al.* (GAMBIT Collaboration), Global fits of GUT-scale SUSY models with GAMBIT, Eur. Phys. J. C **77**, 824 (2017).
[116] P. Bechtle, S. Heinemeyer, O. Stäl, T. Stefaniak, and G. Weiglein, HiggsSignal: Confronting arbitrary Higgs sectors with measurements at the Tevatron and the LHC, Eur. Phys. J. C **74**, 2711 (2014).
[117] O. Stäl and T. Stefaniak, Constraining extended Higgs sectors with HiggsSignal, Proc. Sci. EPS-HEP2013 (**2013**) 314.
[118] P. Bechtle, S. Heinemeyer, O. Stäl, T. Stefaniak, and G. Weiglein, Probing the standard model with Higgs signal rates from the Tevatron, the LHC and a future ILC, J. High Energy Phys. 11 (2014) 039.
[119] P. Bechtle, S. Heinemeyer, T. Klingl, T. Stefaniak, G. Weiglein, and J. Wittbrodt, HiggsSignal-2: Probing new physics with precision Higgs measurements in the LHC 13 TeV era, Eur. Phys. J. C **81**, 145 (2021).
[120] P. Bechtle, O. Brein, S. Heinemeyer, G. Weiglein, and K. E. Williams, HiggsBounds: Confronting arbitrary Higgs sectors with exclusion bounds from LEP and the tevatron, Comput. Phys. Commun. **181**, 138 (2010).
[121] P. Bechtle, O. Brein, S. Heinemeyer, G. Weiglein, and K. E. Williams, HiggsBounds 2.0.0: Confronting neutral and charged Higgs sector predictions with exclusion bounds from LEP and the tevatron, Comput. Phys. Commun. **182**, 2605 (2011).

[122] P. Bechtle, O. Brein, S. Heinemeyer, O. Stal, T. Stefaniak, G. Weiglein *et al.*, Recent developments in HiggsBounds and a preview of HiggsSignal, Proc. Sci. CHARGED2012 (**2012**) 024.

[123] P. Bechtle, O. Brein, S. Heinemeyer, O. Stäl, T. Stefaniak, G. Weiglein, and K. E. Williams, HiggsBounds – 4: Improved tests of extended Higgs sectors against exclusion bounds from LEP, the tevatron and the LHC, Eur. Phys. J. C **74**, 2693 (2014).

[124] P. Bechtle, D. Dercks, S. Heinemeyer, T. Klingl, T. Stefaniak, G. Weiglein, and J. Wittbrodt, HiggsBounds-5: Testing Higgs sectors in the LHC 13 TeV era, Eur. Phys. J. C **80**, 1211 (2020).

[125] N. Aghanim *et al.* (Planck Collaboration), Planck 2018 results. VI. Cosmological parameters, Astron. Astrophys. **641**, A6 (2020).

[126] M. Ackermann *et al.* (Fermi-LAT Collaboration), Searching for dark matter annihilation from Milky Way dwarf spheroidal galaxies with six years of Fermi Large Area Telescope Data, Phys. Rev. Lett. **115**, 231301 (2015).

[127] M. Tanabashi *et al.* (Particle Data Group Collaboration), Review of particle physics, Phys. Rev. D **98**, 030001 (2018).

[128] J. E. Camargo-Molina, B. O'Leary, W. Porod, and F. Staub, Vevacious: A tool for finding the global minima of one-loop effective potentials with many scalars, Eur. Phys. J. C **73**, 2588 (2013).

[129] C. K. Khosa, S. Kraml, A. Lessa, P. Neuhuber, and W. Waltenberger, SModelS database update v1.2.3, Lett. High Energy Phys. **2020**, 158 (2020).

[130] G. Aad *et al.* (ATLAS Collaboration), Search for charginos and neutralinos in final states with two boosted hadronically decaying bosons and missing transverse momentum in pp collisions at $\sqrt{s} = 13$ TeV with the ATLAS detector, Phys. Rev. D **104**, 112010 (2021).

[131] M. Drees, H. Dreiner, D. Schmeier, J. Tattersall, and J. S. Kim, CheckMATE: Confronting your favourite new physics model with LHC data, Comput. Phys. Commun. **187**, 227 (2015).

[132] D. Dercks, N. Desai, J. S. Kim, K. Rolbiecki, J. Tattersall, and T. Weber, CheckMATE 2: From the model to the limit, Comput. Phys. Commun. **221**, 383 (2017).

[133] J. S. Kim, D. Schmeier, J. Tattersall, and K. Rolbiecki, A framework to create customised LHC analyses within CheckMATE, Comput. Phys. Commun. **196**, 535 (2015).

[134] J. Cao, J. Lian, Y. Pan, Y. Yue, and D. Zhang, Impact of recent $(g-2)_\mu$ measurement on the light CP-even Higgs scenario in general next-to-minimal supersymmetric standard model, J. High Energy Phys. 03 (2022) 203.

[135] J. Cao, J. Li, Y. Pan, L. Shang, Y. Yue, and D. Zhang, Bayesian analysis of sneutrino dark matter in the NMSSM with a type-I seesaw mechanism, Phys. Rev. D **99**, 115033 (2019).

[136] CMS Collaboration, Search for a new resonance decaying to two scalars in the final state with two bottom quarks and two photons in proton-proton collisions at $\sqrt{s} = 13$ TeV, HAL (Hyper Articles en Ligne), https://hal.science/hal-03853275.